*International Geology Review*, Vol. 49, 2007, p. 681–716.
Copyright © 2007 by V. H. Winston & Son, Inc. All rights reserved.

# Early Paleozoic Tectonic and Thermomechanical Evolution of Ultrahigh-Pressure (UHP) Metamorphic Rocks in the Northern Tibetan Plateau, Northwest China

AN YIN,[1]

*Department of Earth and Space Sciences, University ofCalifornia, Los Angeles, California 90095-1567; Institute of Geophysics and Planetary Physics, University of California, Los Angeles, California 90095-1567; and Structural Geology Group, China University of Geosciences, Beijing, China*

CRAIG E. MANNING, OSCAR LOVERA, CARRIE A. MENOLD,

*Department of Earth and Space Sciences, University of California, Los Angeles, California 90095-1567*

XUANHUA CHEN,

*Institute of Geomechanics, Chinese Academy of Geological Sciences, Beijing 100085, People's Republic of China*

AND GEORGE E. GEHRELS

*Department of Geosciences, University of Arizona, Tucson, Arizona 85721-0077*

## Abstract

Coesite- and diamond-bearing ultrahigh-pressure (UHP) metamorphic rocks represent continental materials that were once subducted to depths of >90 km. Identifying how these rocks were subsequently returned to Earth's surface has been a major challenge. Opinions on this matter vary widely, ranging from vertical extrusion of a coherent continental slab to channel flow of tectonically mixed mélange. To address this problem, we conducted integrated research across the North Qaidam UHP metamorphic belt using structural mapping, petrologic studies, and geochronologic and thermochronologic analyses. Our regional synthesis indicates that the early Paleozoic Qilian orogen, within which the North Qaidam UHP metamorphic belt was developed, was created by protracted southward oceanic subduction. The process produced a wide mélange belt and the Qilian magmatic arc. Arc magmatism was active between 520 and 400 Ma, coeval with North Qaidam UHP metamorphism. The North Qaidam UHP metamorphic belt also spatially overlaps the early Paleozoic Qilian magmatic arc. Petrologic, geochronologic, and geochemical studies indicate that the protolith of the UHP metamorphic rocks was a mixture of continental and mafic/ultramafic materials, derived either from oceanic mélanges or pieces of a rifted continental margin tectonically incorporated into an oceanic subduction channel. These observations require that the North Qaidam UHP metamorphic rocks originated at least in part from continental crust that was subducted to mantle depths and then transported across a mantle wedge into a coeval arc during oceanic subduction. Upward transport of the UHP rocks may have been accommodated by rising diapirs launched from a mélange channel on top of an oceanic subducting slab. To test this hypothesis, we developed a quantitative model that incorporates existing knowledge on thermal structures of subduction zones into the mechanics of diapir transport. Using this model, we are able to track P-T and T-t paths of individual diapirs and compare them with the observed P-T and T-t paths from North Qaidam. The main physical insight gained from our modeling is that the large variation of the observed North Qaidam P-T paths can be explained by a combination of temporal and spatial variation of thermal structure and mechanical strength of the mantle wedge above the early Paleozoic Qilian subduction slab. Hotter P-T trajectories can be explained by a high initial temperature (~800°C) of a diapir that travels across a relatively strong mantle wedge (i.e., activation energy E = 350 kJ/mol for dry olivine), while cooler P-T paths may be explained by a diapir with initially low temperature (~700°C) that traveled through a weaker mantle wedge, with its strength at least two orders of magnitude lower than that of dry olivine. This latter condition could have been achieved by hydraulic weakening of olivine aggregates in the mantle wedge via fluid percolation through the mantle wedge during oceanic subduction.

[1]Corresponding author; email: yin@ess.ucla.edu

## Introduction

ONE OF THE MOST important geologic discoveries in the past three decades is the recognition of coesite- and diamond-bearing ultrahigh-pressure (UHP) metamorphic rocks in continental crust (e.g., Chopin, 1984, 2003; Smith, 1984; Coleman and Wang, 1995; Hacker and Liou, 1998; Ernst and Liou, 2000a; Liou et al., 2004). The UHP metamorphic rocks represent continental materials that were once carried to depths of >90 km and were subsequently exhumed to shallow crustal levels (e.g., Ernst and Liou, 2000b). The deep burial and subsequent exhumation processes of UHP metamorphic rocks provide important information about the dynamics of continental-lithosphere deformation and its interaction with asthenospheric flow (e.g., van den Buekel, 1992; Davies and van Blanckenburg, 1995; Ernst and Liou, 1995; van Blanckenburg and Davies, 1995; Chemenda et al., 1996, 2000; Ranalli et al., 2000; Gerya and Yuan, 2003; Gerya et al., 2004). A fundamental requirement for understanding the mechanisms of UHP metamorphism is the determination of tectonic settings under which the associated metamorphic rocks were produced. In the past two decades, two main classes of tectonic models to explain UHP metamorphism have emerged: (1) the Himalayan-style model (Liou et al., 2004) that emphasizes the role of contraction during continent-continent collision in causing UHP metamorphism; and (2) the oceanic-subduction model that requires UHP metamorphism to occur during oceanic subduction and arc magmatism (Fig. 1).

The Himalayan-style model is based on the observation that UHP metamorphic rocks commonly occur in continent-continent or continent-arc collisional orogens (e.g., Coleman and Wang, 1995) and have P-T paths characteristic of oceanic subduction zones (e.g., Ernst and Peacock, 1996). This has led many workers to attribute UHP metamorphism to subduction of coherent sections of continental lithosphere to mantle depths (e.g., Liou et al., 1996; Hacker et al., 2000, 2005). The Himalayan-style model may be further divided into sub-models based on the predicted geologic processes and related exhumation: (1) channel flow during continental subduction (Mancktelow, 1995; Dobretsov, 2000); (2) diapiric flow of subducted continental materials at the terminal stage of continent-continent collision (Cloos, 1993; Wang and Cong, 1999; Hacker et al., 2005); (3) large-scale intracontinental thrusting and coeval erosion (Okay and Sengör, 1992; Yin and Nie, 1993, 1996; Nie et al., 1994); (4) pure-shear crustal thickening and exhumation during continent-continent collision (Dewey et al., 1993; Ryan, 2001; Gilotti and Ravna, 2002); and (5) wedge extrusion induced by break off of oceanic slabs and subsequent upward motion of deeply subducted continental crust (van den Buekel, 1992; Ernst and Liou, 1995; Davies and van Blanckenburg, 1995; van Blanckenburg and Davies, 1995; Chemenda et al., 1996) (Fig. 1). Noting coeval UHP metamorphism and arc magmatism in some orogenic belts, a few workers have suggested that UHP metamorphism could result from oceanic subduction of mélange materials that were exhumed later by corner flow or diapiric ascent (Lardeaux et al., 2001; Yin et al., 2001) (Fig. 1).

The above tectonic models make specific predictions about the temporal relationship between UHP metamorphism and arc magmatism, exhumation mechanism (i.e., erosion versus tectonic denudation), P-T paths, protolith of UHP metamorphic rocks, residence time of UHP metamorphic rocks in the lower crust, and the mode and kinematic history of deformation associated with prograde and retrograde metamorphism (Table 1). For example, the wedge extrusion model (1E in Fig. 1), widely used to explain the evolution of UHP metamorphic terranes around the world (Dabie Shan: Maruyama et al., 1994; Liou et al., 1996; Hacker et al., 2000; Himalaya: de Sigoyer et al., 2000; Chemenda et al., 2000; O'Brien et al., 2001; Kohn and Parkinson, 2002; Leech et al., 2005; Kokchetav, northern Kazakhstan: Kaneko et al., 2000; and North Qaidam: Yang et al., 2001; Song et al., 2005, 2006), makes the following predictions: the UHP terrane should be located on the passive continental margin of the subducting plate (e.g., O'Brien et al., 2001); the exhumed UHP metamorphic terrane should have preserved the geochemical and geochronologic signatures of the down-going continental lithosphere (e.g., Jahn, 1999); extrusion of the crustal wedge should be accommodated by coeval normal and thrust faulting (Ernst and Liou, 1995); UHP metamorphism should postdate the initial ocean closure and thus arc magmatism (Hacker et al., 2000); and the residence time of the UHP metamorphic rocks in the lower crust should be short and no longer than a few million years (e.g., de Sigoyer et al., 2000; Leech et al., 2005). As shown in this paper, the wedge extrusion model cannot explain the geologic observations from the North Qaidam UHP metamorphic belt. Instead, the petrologic, structural, and

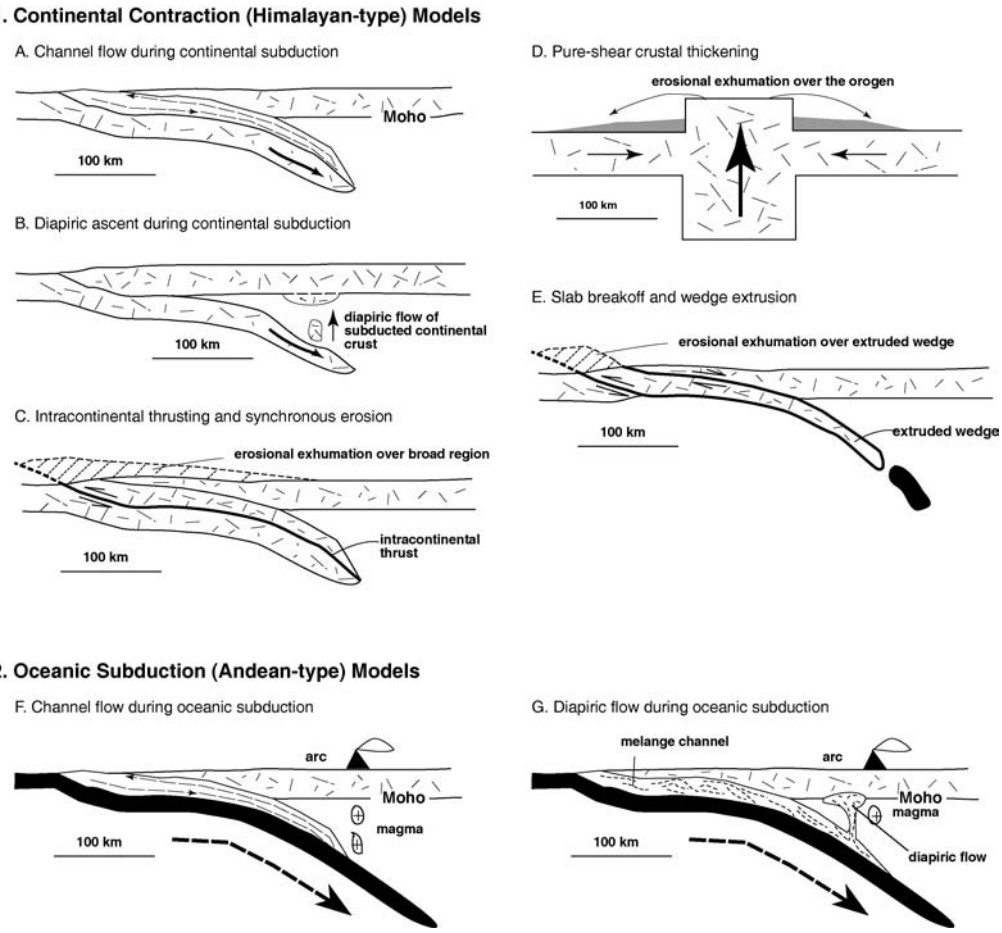


FIG. 1. Tectonic models for ultrahigh-pressure metamorphism. A. Channel flow during continental subduction (Mancktelow, 1995; Dobretsov, 2000). B. Diapiric ascent of subducted continental materials during continental collision (Cloos, 1993; Wang and Cong, 2000). C. Intracontinental thrusting (Okay and Sengör, 1992; Yin and Nie, 1993; Nie et al., 1994). D. Pure-shear crustal thickening during continental collision (Dewey et al., 1993; Ryan, 2001). E. Breakoff of oceanic slab and subsequent wedge extrusion during continental subduction (Ernst and Liou, 1995; Davies and van Blanckenburg, 1995; van Blanckenburg and Davies, 1995). F. Occurrence of UHP metamorphism by channel flow during oceanic subduction (Lardeaux et al., 2001). G. Diapiric ascent and final emplacement of subducted mélange materials onto the base of a magmatic arc during oceanic subduction (Yin et al., 2001).

geochronologic data support a new mechanism that favors diapiric flow of subducted oceanic mélanges across the mantle wedge and their subsequent ponding in the lower crust of a coeval arc during oceanic subduction.

## Deformation History of Northern Tibet

The North Qaidam UHP metamorphic belt is an integral part of the early Paleozoic Qilian orogenic system in northern Tibet (Zhang et al., 1984; Hsu et al., 1995; Yin and Nie, 1996; Sengör and Natal'in, 1996; Sobel and Arnaud, 1999; Gehrels et al., 2003a, 2003b; Yin et al., 2002) (Fig. 2). Due to the Cenozoic Indo-Asian collision and Mesozoic intracontinental deformation, the original configuration of the Paleozoic Qilian orogen has been significantly modified (Yin and Harrison, 2000; Chen et al., 2003; Gehrels et al., 2003a, 2003b). As a result, understanding the evolution of the early Paleozoic

TABLE 1. Predictions of Major Tectonic Models for UHP Metamorphism

| Prediction | Temporal relation to arc magmatism | Style of exhumation | Tectonic setting | P-T paths | Protolith of UHP rocks | Residence time in the lower crust | Deformation style and history |
|---|---|---|---|---|---|---|---|
| Channel flow during continental subduction | Post-arc magmatism | Localized along sutures syn-UHP metamorphism, and/or intracontinental thrusts | Collisional orogens | Uniform P-T path | Continental protoliths | A few m.y. | Ductile deformation associated with tectonic mixing |
| Diapiric flow during continental subduction | Post-arc magmatism | No exhumation required during UHP metamorphism | Collisional orogens | Diverse P-T path due to different diapir sizes and thermal structures | Continental protoliths | 10s of M.y. | UHP rocks intrudes into lower and middle crustal rocks |
| Intra-continental thrusting | Post-arc magmatism | Exhumation over wide region in over-riding thrust plates | Collisional orogens | Uniform P-T path | Continental protoliths | A few to ~10 m.y. for plate tectonic rate of thrusting | Coherent crustal section with UHP rocks thrusting over low-grade rocks |
| Pure-shear crustal thickening | Post-arc magmatism | Exhumation of UHP rocks within collisional orogens | Collisional orogens | Uniform P-T path | Continental protoliths | A few to ~10 m.y. for plate tectonic rate of convergence | Distributed crustal shortening |
| Wedge extrusion due to slab breakoff | Post-arc magmatism | Localized exhumation in the downgoing continental crust below sutures | Collisional orogens | Uniform P-T path | Continental protoliths | A few m.y. | Coeval thrust and normal faulting in the downgoing continental crust |
| Channel flow during oceanic subduction | Syn-arc magmatism | Localized exhumation in accretionary complexes | Active oceanic convergent margins | Uniform P-T path | Oceanic and continental protoliths | A few m.y. | Ductile deformation associated tectonic mixing |
| Diapiric flow during oceanic subduction | Syn-arc magmatism | No exhumation required during UHP metamorphism | Active oceanic convergent margins | Diverse P-T paths due to different diapir sizes and thermal structures | Oceanic and continental protoliths | 10s of m.y. | UHP rocks occur within magmatic arcs |

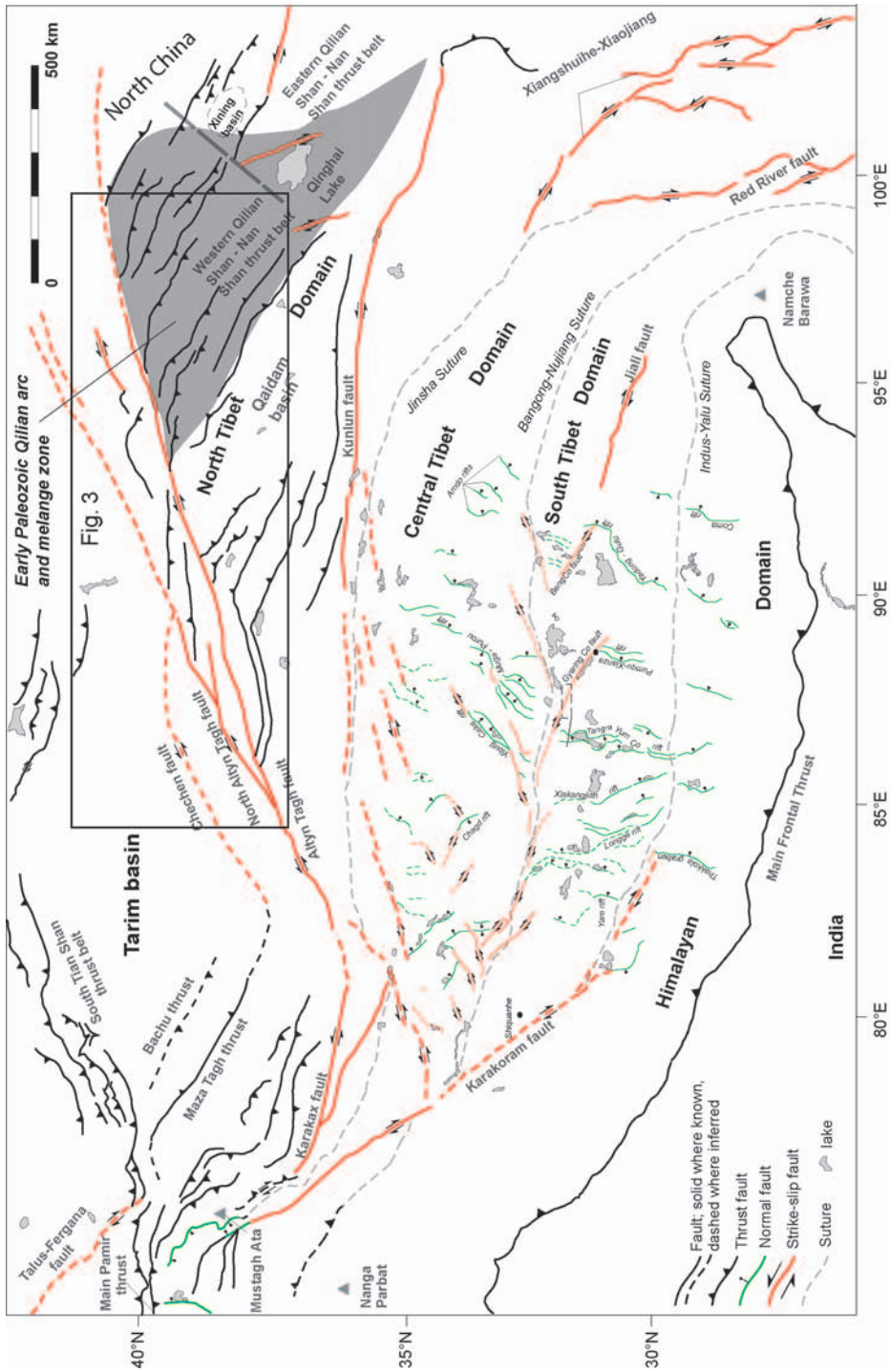


FIG. 2. Cenozoic tectonic map of the Himalayan-Tibetan orogen and the location of the Qilian Shan–Nan Shan thrust belt, modified from Taylor et al. (2003). The early Paleozoic Qilian orogen spatially overlaps the Cenozoic Qilian Shan–Nan Shan thrust belt.

Qilian orogen requires a detailed knowledge of Cenozoic and Mesozoic deformation history and their effects on Paleozoic structures.

*Cenozoic tectonics*

The Cenozoic Qilian Shan–Nan Shan thrust belt is the dominant tectonic feature of northern Tibet and an integral part of the overall Cenozoic Himalayan-Tibetan orogen (Fig. 2). The belt is bounded by the Altyn Tagh fault to the northwest and the Xining basin to the northeast (Fig. 2) (Burchfiel et al., 1989; Cui et al., 1998; Meyer et al., 1998). Along a NW-trending line passing the western edge of the Qinghai Lake, the deformation style of the thrust belt changes drastically (Fig. 2). To the west, the thrust belt is thin-skinned in style and thrusts are closely spaced (20–30 km; Meyer et al., 1998). In contrast, the eastern thrust belt is thick-skinned and thrusts are widely spaced (>50 km) (Liu, 1988; Burchfiel et al., 1989; Wang and Burchfiel, 2004) (Fig. 2).

The southwestern part of the Qilian Shan–Nan Shan thrust belt initiated at ~50 Ma (Huang et al., 1996; Jolivet et al., 2001; Yin et al., 2002), whereas in the northwest the thrusts began either at ~30 Ma or younger around 16 Ma (Yin et al., 2002; cf. Wang, 1997; Gilder et al., 2001; Wang et al., 2003). Along the northern edge of the thrust belt, Cenozoic contraction may have started at ~20 Ma (George et al., 2001). In the east, Cenozoic thrusting began at or before ~29 Ma in the Linxia basin in the northeastern corner of the Tibetan Plateau (Fang et al., 2003) and in the Pliocene (~6 Ma) in the Guide-Gonghe basin immediately east of the Qaidam basin (Pares et al., 2003).

The Altyn Tagh fault that bounds the Qaidam basin and the Qilian Shan–Nan Shan thrust belt may have initiated at ~50–45 Ma; it also has variable amounts of left-slip motion due to thrust branching from strike-slip fault strands, multiple stages of lengthening of existing strands, and nucleation of new strands during the Indo-Asian collision (Bally et al., 1986; Yin and Nie, 1996; Wang, 1997; Meyer et al., 1998; Yue and Liou, 1999; Yin et al., 2002; Yue et al., 2001; Darby et al., 2005). The maximum amount of estimated left-slip displacement on the Altyn Tagh fault varies from ~1200 km to <100 km (CSBS, 1992; Wang, 1997), but the most robust determination falls in the range of 550 to 350 km (Ritts and Biffi, 2000; Cowgill, 2001; Yang et al., 2001; Cowgill et al., 2003; Gehrels et al., 2003a, 2003b; Yue et al., 2004). One of the offset markers across the Altyn Tagh fault is the NW-trending North Qaidam UHP metamorphic belt that may have been offset for ~450 km (Fig. 3) (Yang et al., 2001; Zhang et al., 2001). However, this offset estimate is problematic because the location of the UHP belt is controlled by Cenozoic thrusts along the northern margin of the Quidam basin, which were developed coeval with, rather than prior to, motion on the Altyn Tagh fault.

The Qaidam basin is the largest intermontane basin inside the Tibetan Plateau and has preserved a complete record of Cenozoic sedimentation locally exceeding 7 km (Bally et al., 1986; Song and Wang, 1993; Huang et al., 1996; Zhang, 1997; Yin et al., 2002; Rieser et al., 2005) (Fig. 3). The basin is triangular in shape and is bounded by the left-slip Altyn Tagh fault in the northwest, the Qilian Shan–Nan Shan thrust belt in the northeast, and the Qimen Tagh–Eastern Kunlun thrust belt in the south (Meyer et al., 1998). The Cenozoic origin of the Qaidam basin has been related to the development of a large synclinorium (Bally et al., 1986), discrete and stepwise growth of the Tibetan Plateau (Meyer et al., 1998), development of a fold belt along a mid-crustal detachment (Burchfiel et al., 1989), and progressive closure of an internally drained basin due to offset of a topographic high along the Altyn Tagh fault (Yin et al., 2002). Along the northern edge of the Qaidam basin, Cenozoic strata are juxtaposed by a series of north-dipping thrusts below Ordovician metasedimentary and metavolcanic rocks and high-grade gneisses including eclogite-bearing UHP rocks (Fig. 7).

*Mesozoic tectonics*

Due to limited exposure of Mesozoic rocks in northern Tibet, the geologic history of this period is not well constrained. Geologic studies based on stratigraphic and sedimentologic arguments alone have led to the conclusion that northern Tibet experienced intense Jurassic N-S contraction (e.g., Huo and Tan, 1995), possibly related to collision between Asia and the Qiangtang terrane and Asia and the Lhasa terrane (Ritts and Biffi, 2000). In contrast, structural mapping, examination of growth-strata relationships, thermochronologic studies, and subsidence analysis of sedimentary basins led others to suggest that the northern Tibetan Plateau experienced several phases of extension between the latest Triassic and the Early Cretaceous (Huo and Tan, 1995; Huang et al., 1996; Sobel, 1999; Vincent and Allen, 1999; Kapp et al., 2000, 2003b; Chen et al., 2003). At least

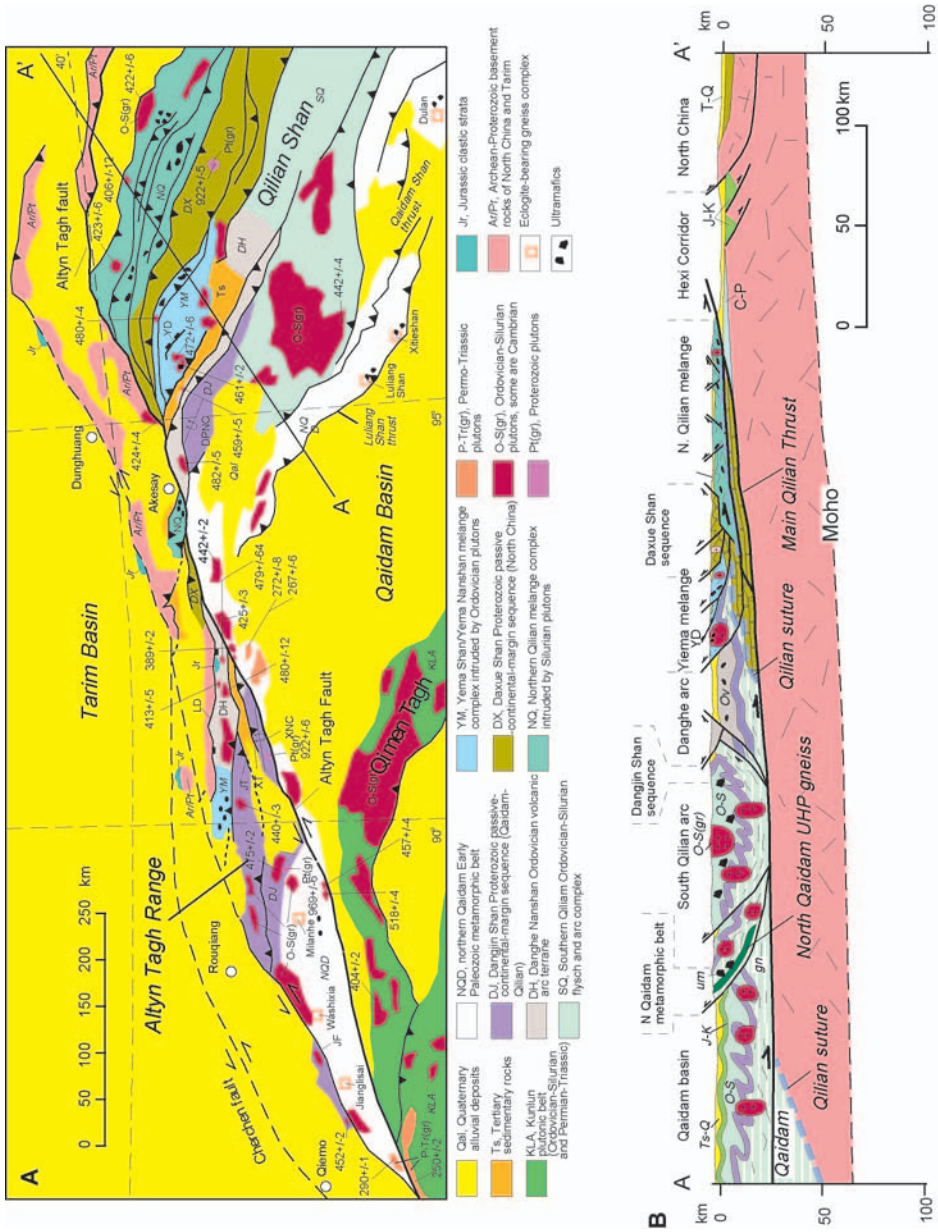


FIG. 3. A. Tectonic map of the Qilian Shan–Nan Shan region (modified from Yin et al., 2002) and distribution of U-Pb ages of major granitoids from Cowgill et al. (2003) and Gehrels et al. (2003a). B. Geologic cross section across the Qilian Shan–Nan Shan thrust belt showing the relationship between the Paleozoic lithologic units and Cenozoic structures. Note that the central Qilian Shan passive continental margin sequence is part of the North China craton that is brought up to surface by Cenozoic thrust.

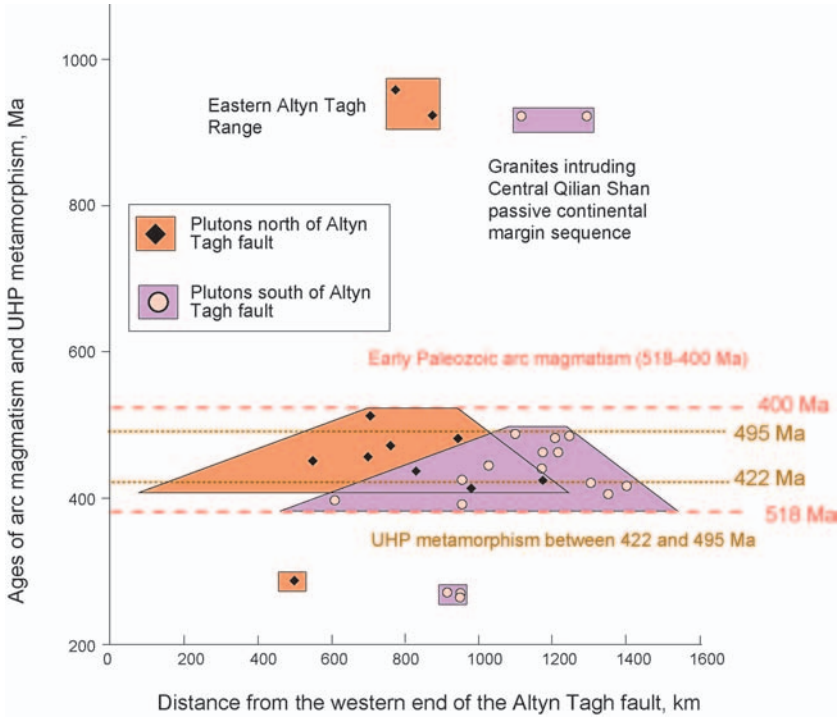


FIG. 4. Age distribution of granitoids across the Qilian Shan, Nan Shan, and Altyn Tagh Range on both sides of the Altyn Tagh fault. Data compiled from Gehrels et al. (2003a) and Cowgill et al. (2003) and sample locations are indicated in Figure 3A.

locally, Mesozoic normal faults were reactivated by Cenozoic contraction, produced locally younger-over-older relationships across Cenozoic thrusts (Chen et al., 2003).

*Paleozoic tectonics*

The effect of early Paleozoic tectonics in northern Tibet is best expressed by the development of the Qilian orogen, which resulted from closure of a complex Qilian ocean between the North China craton to the north and the Kunlun continental (?) arc to the south. The orogen in present map view shows a systematic decrease in width from west to east (Fig. 2), an observation that is important to our interpretation for the emplacement mechanism of the North Qaidam UHP metamorphic rocks. The Qilian orogen exposes lower Paleozoic flysch sequences, arc complexes, and low- to high-grade metamorphic rocks (Li et al., 1978; Liu, 1988; Gansu BGMR, 1991; Qinghai BGMR, 1991; Yin and Nie, 1996) (Fig. 3). In general, the Qilian Shan–Nan Shan region consists of three tectonostratigraphic belts with a Proterozoic passive continental margin sequence in the central part (the Daxue Shan Sequence) sandwiched between mélange belts to the north (North Qilian) and to the south (North Qaidam), respectively (Yang et al., 2001; Gehrels et al., 2003a, 2003b; Song et al., 2005, 2006; Zhang et al., 2005). Three phases of magmatism have been documented in the Qilian Shan, Nan Shan, and Qaidam regions (Cowgill et al., 2003; Gehrels et al., 2003a, 2003b): (1) at 960–920 Ma as small and isolated plutons that only intrude Proterozoic passive continental margin sequences along the southern edge of the North China craton; (2) at 520–400 Ma as arc-related plutons and volcanic complexes; and (3) at ~270 Ma as isolated plutons of the Permian Kunlun arc (Fig. 4). As shown below, the early Paleozoic arc magmatism was coeval with—and spatially overlapping—UHP metamorphism in the North Qaidam region.

Influenced by the early syntheses of Li et al. (1978) and Zhang et al. (1984), many geologists working in northern Tibet held the view that the Qilian orogen was created by the closure of two oceans on the north and south sides of a microconti-

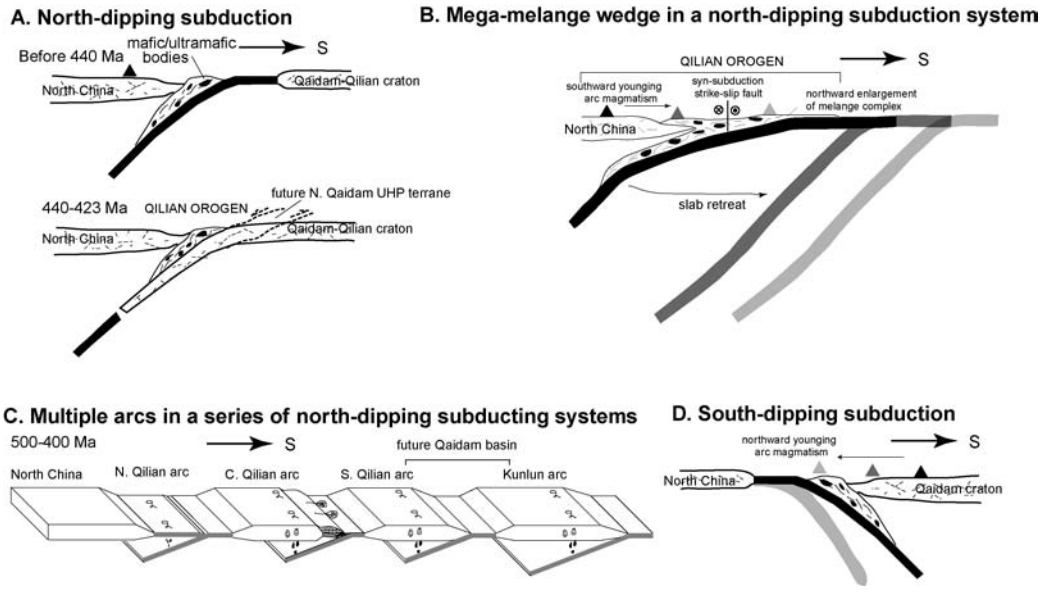


FIG. 5. Major tectonic models for the development of the early Qilian orogen. A. Microcontinental model. B. Mega-accretionary wedge model. C. Multiple arc collision model. D. Single north-dipping subduction zone model. See text for detailed discussion of the validity of each model and their predictions.

nent in the central Qilian region. This is expressed by the exposure of two subparallel suture zones dividing the Qilian orogen into five tectonic belts from north to south: (1) a continental arc along the southern edge of the North China craton; (2) a suture generated by both south-and north-dipping subduction; (3) the central Qilian microcontinental block in the middle; (4) a suture zone along the northern edge of the Qaidam basin generated by north-dipping subduction; and (5) the Qaidam microcontinent (e.g., Yang et al., 2001; also see Song et al., 2005 for a complete review of this tectonic concept) (Fig. 5A). This model requires that North Qaidam UHP metamorphism occurred in the Qaidam continental crust.

Widespread ultramafic fragments and flysch complexes across the Paleozoic Qilian orogen led Sengör and Natal'in (1996) to suggest that the entire orogen was built by the development of an evolving mélange complex, which was enlarged by both tectonic accretion and strike-slip faulting during oceanic subduction. As the mélange complex grew, the related magmatic arc migrated southward (Fig. 5B). This provocative hypothesis explains several puzzling features across the Qilian orogen: (1) the lack of coherent stratigraphic sequences for pre-Devonian strata; (2) lack of any signs of Precambrian basement rocks within the Qilian orogen north of Daqaidam Shan; (3) widely mixed lithology including ultramafic rocks; and (4) an unusually wide mélange complex zone that exceeds 600 km even before taking account of Cenozoic shortening (Fig. 3).

In addition to the microcontinent and mega-accretionary wedge models, there are two other competing models for the development of the Qilian orogen: (1) the orogen was produced by collision of multiple island arcs and micro-continental blocks with the Tarim–North China craton (Li et al., 1978; Hsü et al., 1995; Yin and Nie, 1996; Yin and Harrison, 2000) (Fig. 5C); and (2) the orogen was created by arc-continent collision along a single southward subduction zone (Sobel and Arnaud, 1999; Gehrels et al., 2003a, 2003b) (Fig. 5D). In the multiple-arc model, a major suture should be present along the northern margin of the Qaidam basin and the main body of the Qilian Shan–Nan Shan region should be a micro-continental block. This model does not explain the observation that deformation is penetrative and ophiolitic fragments are widely distributed across the Qilian orogen. In the second model, the Qilian Shan–Nan Shan region is required to be a single and long evolving arc built on the northern edge of the Qaidam microcontinent that eventually collided with the North China craton. This model

has the advantage of explaining the width of the Qilian orogen, which is greater than typical accretionary wedges (<200 km, see Sengör and Natal'in, 1996 for detailed discussion and their special plea for synsubduction strike-slip faulting to duplicate the arc). However, the same observation could also be explained by multiple accretion of arcs onto the North China craton or the Qaidam block during the closure of the Qilian ocean.

A major problem with the above tectonic models for the early Paleozoic evolution of the Qilian orogen is that they neglect the effect of large-magnitude Mesozoic and Cenozoic deformation, which must have redistributed early tectonic elements. First, the Triassic collision between the North and South China blocks may have caused westward extrusion of the Qaidam block for several hundreds of kilometers along right-slip faults in the north and left-slip faults in the south (Yin and Nie, 1996). Second, Cenozoic shortening with a magnitude of >230 km may have accumulated across the Qilian Shan—Nan Shan thrust belt (Yin and Harrison, 2000). Considering these effects may help explain some of the puzzling relationships of the Qilian orogen. For example, a Proterozoic passive continental margin sequence is present in the central Qilian region surrounded by oceanic mélange complexes (Fig. 3). This observation has been used as evidence for the presence of a microcontinent within the Qilian orogen (e.g., Li et al., 1978; Yang et al., 2001). However, the lack of Paleozoic magmatism in the inferred continental arc invalidates this interpretation (Gehrels et al., 2003a) (Fig. 3). On the other hand, the close correlation of Cenozoic structures and the distribution of pre-Cenozoic lithologic units in the Qilian Shan region require strong control by the Paleozoic tectonic framework over Cenozoic deformation.

A possible interaction between the Paleozoic and Cenozoic structures is that the early Paleozoic south-dipping mélange channel may have been duplicated by Cenozoic thrusts. This has produced apparently multiple suture zones across the Qilian Shan region, exposing rocks of the North China craton that were originally underthrust below the early Paleozoic mélange belt (Fig. 6) (see Kapp et al., 2003a for a similar case in southern Tibet). Based on this interpretation, we propose a six-stage evolutionary model for the geologic history of the Qilian Shan–Nan Shan region (Fig. 6). *Stage 1 (900–600 Ma)*: Development of passive continental margins on both sides of the Kunlun-Qaidam microcontinent. *Stage 2 (520–400 Ma)*: South-dipping subduction of the Qilian oceanic plate and development of the Qilian arc. A large accretionary wedge was developed along the northern margin of the Kunlun-Qaidam microcontinent that was enlarging northward associated with northward migration of the magmatic front from ~510 Ma in the south to ~400 Ma along the northern edge of the Qilian orogen. *Stage 3 (400–375 Ma)*: Collision between the Qilian arc and North China associated with obduction of the Qilian mélange complex over the North China passive continental margin. *Stage 4 (230–100 Ma)*: Episodic extension producing extensional basins in a back-arc setting from the Late Triassic to Early Cretaceous. *Stage 5 (50–40 Ma)*: Initiation of Indo-Asian collision and contractional deformation in the Qilian Shan-Nan Shan region. *Stage 6 (40–0 Ma)*: Duplication of the early mélange channel by Cenozoic imbricate thrusts, which locally brought up the passive continental margin sequence of the North China craton.

Our proposed model adopts some elements of the Sengör and Natal'in (1996) hypothesis, such as assuming the Qilian orogen to have been constructed over a single mélange complex, and the Qilian arc magmatism to have been constructed mostly over an oceanic crust and an evolving mélange complex (Fig. 6). However, the polarity of oceanic subduction in our model is opposite that suggested in the Sengör and Natal'in (1996) hypothesis, but similar to the south-dipping subduction models of Sobel and Arnoud (1999) and Gehrels et al. (2003a). Additionally, we suggest that the apparent duplication of early Paleozoic arcs was caused by Cenozoic thrusting of a subduction channel rather than by syn-subduction Paleozoic strike-slip faulting as anticipated by Sengör and Natal'in (1996).

## Geology of the North Qaidam Metamorphic Belt

North Qaidam UHP metamorphic rocks are exposed in the Luliang Shan, Xitie Shan, and Dulan areas along a 450 km long belt (Fig. 3) (e.g., Yang et al. 2000, 2001; Manning et al., 2001; Menold et al., 2001, 2003a; Song et al., 2003, 2005, 2006; Zhang et al., 2005). The location of this metamorphic belt is controlled by a Cenozoic thrust system coeval with motion on the Altyn Tagh fault (Yin et al., 2002). Each UHP terrane has a width of 15–50 km in the N-S direction and ~50–100 km E-W. Because the

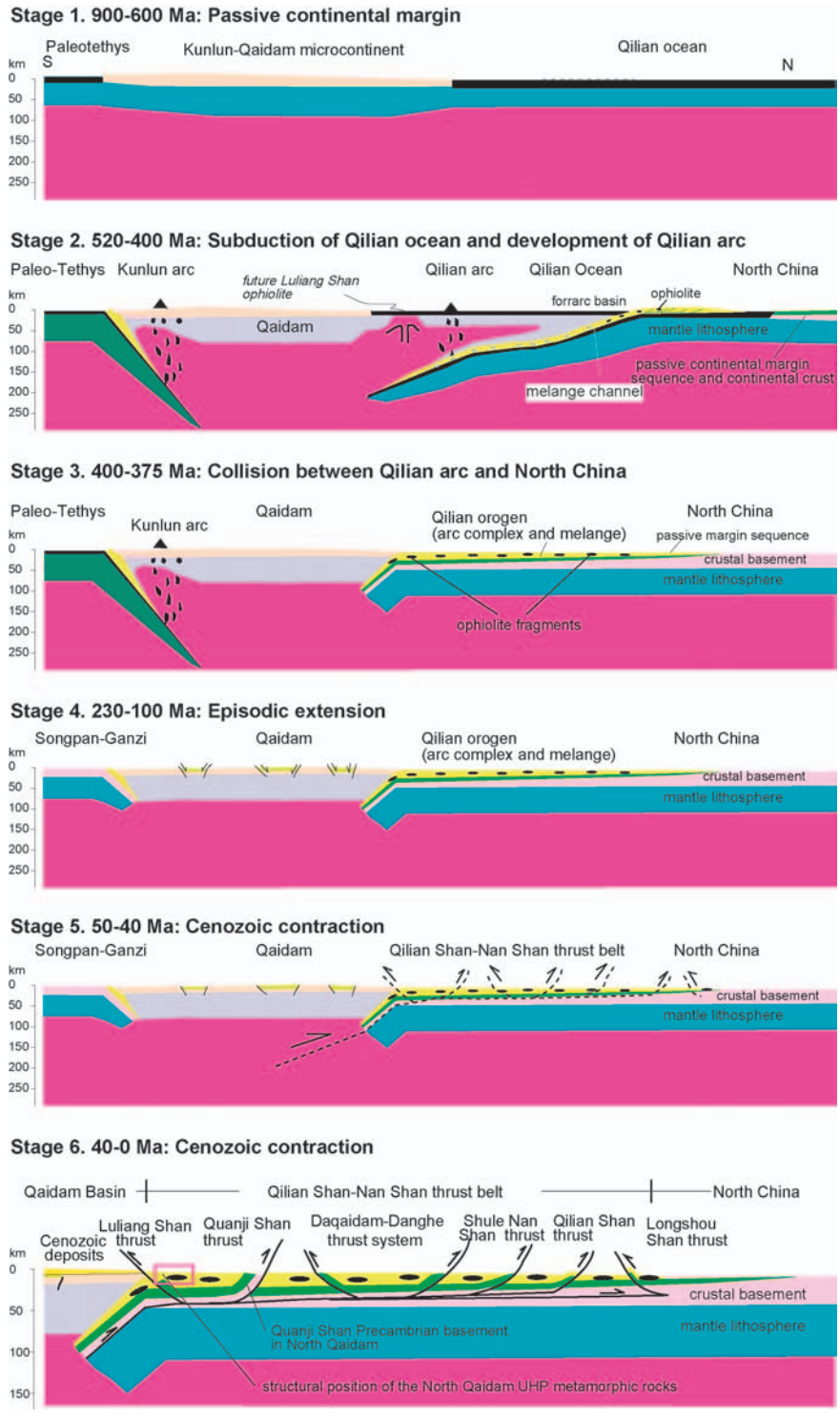


FIG. 6. Tectonic evolution of the early Paleozoic Qilian orogen and the Kunlun arc.

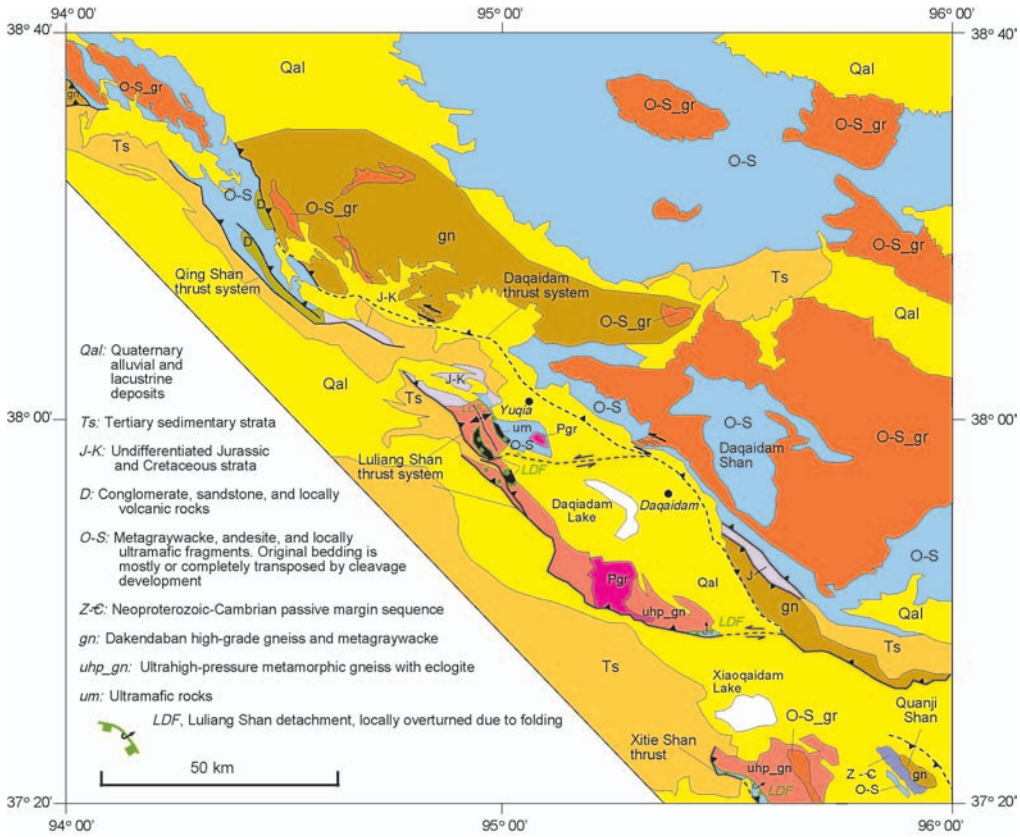


FIG. 7. Geologic map of the western North Qaidam UHP metamorphic belt, simplified from Qinghai BGMR (1993), and based on our own field observations.

UHP metamorphic belt is bounded in the north and south by a north-dipping Cenozoic thrust, the exposed width of the North Qaidam UHP belt represents only a small fraction of its original size (Fig. 3).

### *Lithology*

The North Qaidam area exposes high- and low-grade metamorphic rocks that include Precambrian (?) gneisses overlain by Neoproterozoic–Cambrian (?) strata (Qinghai BGMR, 1991), UHP metamorphic rocks, and Ordovician–Silurian metagraywacke and metavolcanic rocks (Fig. 7). Unmetamorphosed rocks include Devonian continental deposits (conglomerates, sandstone, and minor volcanic rocks), Carboniferous shallow-marine strata, Permian–Triassic continental sedimentary and volcanic rocks, and Mesozoic and Cenozoic lacustrine and fluvial basin fills (Liu, 1988; Qinghai BGMR, 1991; Yang et al., 2001) (Figs. 3 and 7). The gneisses, including eclogite-bearing UHP metamorphic rocks, are commonly referred to as the Dakendaban Group, and are considered to be the Precambrian basement of the Qaidam basin (e.g., Qinghai BGMR, 1991). This division has two problems. First, recent geochronologic results show that the age of protolith of the Dakendaban rocks are as young as Ordovician (e.g., Song et al., 2005, 2006). Second, our structural mapping (see below) indicates that high-grade metamorphic rocks in the region are located in different structural positions with respect to a regional detachment contact (the Luliang Shan detachment, see below). Because of these, we restrict our usage of the Dakendaban Group only to the gneissic rocks in the hanging wall of the Luliang Shan detachment (Figs. 7, 8A, 8B, and 9).

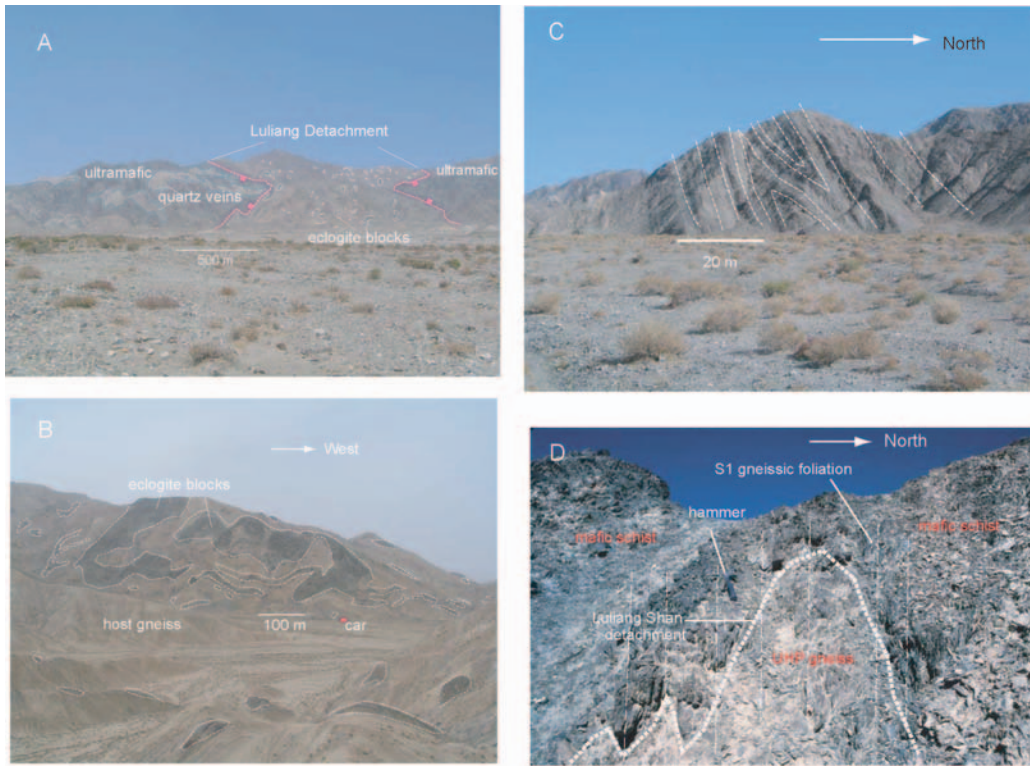


FIG. 8. Field photos from the North Qaidam region. A. Warped Luliang detachment fault juxtaposing mafic schist and ultramafic rocks above and eclogite-bearing UHP metamorphic gneiss below. The antiform is coaxial with Cenozoic folds. B. Isoclinally refolded eclogite sheet in the core of the Luliang Shan Range. Note that the size of eclogite blocks decreases along the fold limbs, possibly due to stretching and internal flow during the emplacement of the UHP metamorphic bodies. C. Isoclinal folds of garnet-bearing metagraywacke in the Dakendaban Group. Note that bedding is completely transposed by folding. D. Tightly folded Luliang Shan detachment separating mafic schist above and UHP gneiss below. Note that gneissic foliation crosscuts the folds and defines the axial surfaces, indicating folding of the fault prior to foliation development.

The original bedding of the metapelite in the Dakendaban Group and the Ordovician–Silurian metasedimentary sequence has been transposed by late development of cleavage and gneissic foliation associated with isoclinal folding (Fig. 8C). In contrast, Devonian and younger strata lack the ductile structural fabrics. This relationship suggests that ductilely deformed Ordovician–Silurian rocks were exhumed to shallow crustal levels prior to the Devonian. Distinction between the Dakendaban gneisses and Ordovician–Silurian metasedimentary and meta-volcanic rocks is not straightforward in the field, inasmuch as both are highly deformed schists and gneisses. The two units may be in gradational contact and together experienced early Paleozoic deformation and metamorphism. The UHP rocks are mostly garnet-bearing quartzofeldspathic gneisses associated with eclogite and garnet peridotite blocks with sizes ranging from a few meters in the longest dimension to several hundreds of meters (Fig. 8B).

Throughout the North Qaidam metamorphic belt, ophiolitic fragments are present in the hanging wall and garnet peridotite in the footwall of the Luliang detachment (Yang et al., 2001; Song et al., 2003, 2005). In the Luliang Shan area, the ophiolite in the detachment hanging wall contains serpentinized peridotite, gabbro, sheeted dikes, and basalt, all of which were penetratively deformed and metamorphosed under epidote-amphibolite facies conditions. Igneous zircons from plagiogranite dikes yield

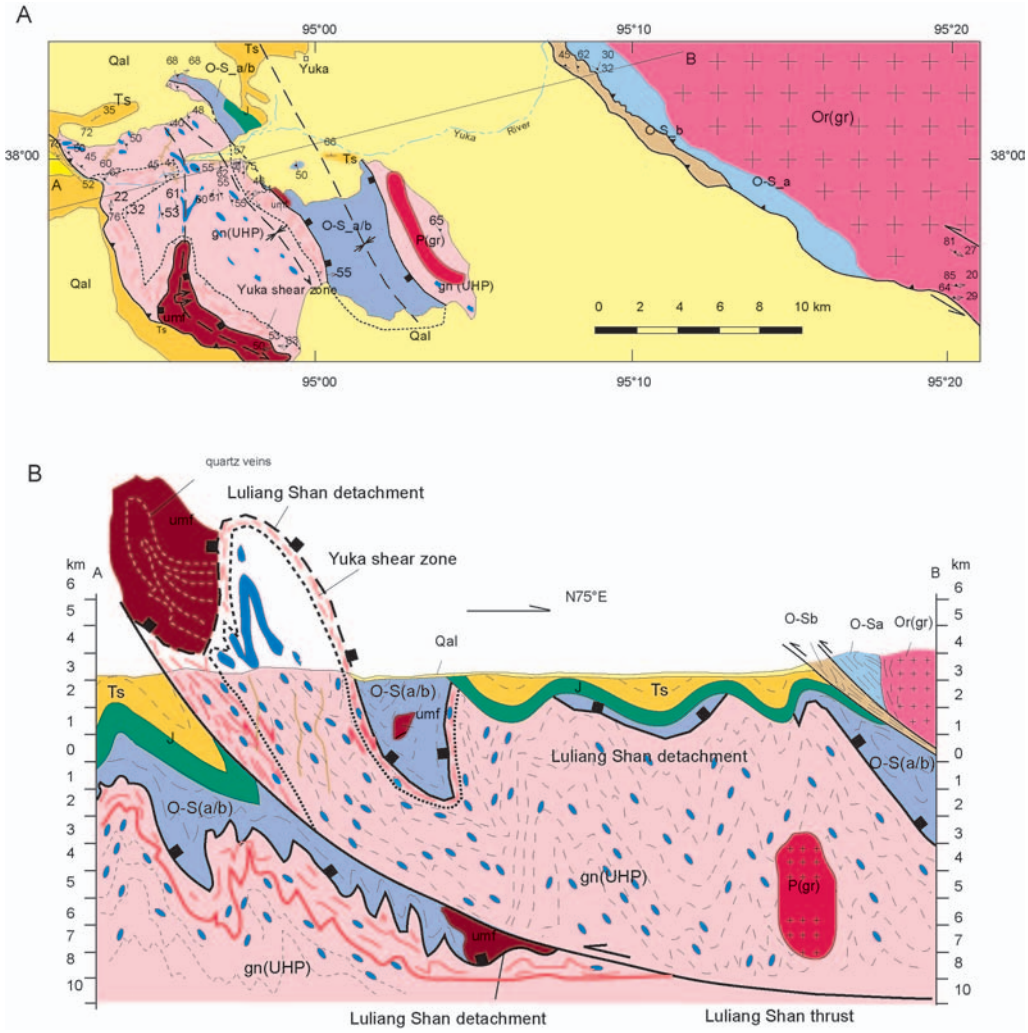


FIG. 9. A. Geologic map of the Luliang Shan area, mostly based on mapping by A. Yin, G. Gehrels, and X. H Chen in 2000 and contribution from C. Menold in 2002 and 2003. Abbreviations: P(gr) = Permian granite; Or(gr) = Ordovician granite; O-S_a = metasedimentary and metavolcanic unit of Ordovician and Silurian sequences; O-S_b = Ordovician–Silurian mafic schist; gn(UHP) = ultrahigh-pressure gneiss; Ts = Tertiary sedimentary strata; J = Jurassic sedimentary strata; um = ultramafic rock. B Geologic cross section of the Luliang Shan.

a U-Pb crystallization age of ~560 Ma (C. Menold, unpubl. data). Thus, closure of the ocean must have postdated this time. Whole-rock geochemistry (C. Menold, unpublished data) suggests a marginal or back-arc setting for the ophiolite. In the context of our proposed tectonic model (Fig. 6) for the evolution of the Qilian orogen, the North Qaidam ultrahigh-pressure metamorphic belt was located along the southernmost part of the Qilian orogen.

*Structural geology*

Major structures in the North Qaidam area may be illustrated by the geology of the Luliang Shan, where we conducted most of our field work (Figs. 7 and 9). Detailed geologic maps, structural analysis, and lithologic description will be presented elsewhere, but we outline some of the first-order observations.

*Cenozoic thrusts and folds*. Major Cenozoic thrusts in the area are north-dipping and bound the southern edges of mountain ranges such as the Qing Shan, Luliang Shan, Xitie Shan, and Daqaidam Shan (Fig. 3A). Some of these structures remain active, such as the Daqaidam thrust that offsets Quaternary alluvial fan surfaces. The thrusts commonly place gneisses and low-grade early Paleozoic metamorphic rocks over Tertiary and Quaternary strata; they die out laterally into folds involving both high-grade gneisses and Mesozoic and Cenozoic sedimentary rocks (Figs. 7 and 9). The coaxial relationship between Cenozoic antiforms and synforms in the UHP gneisses in the Luliang Shan area indicates that the metamorphic gneisses are also folded by Cenozoic deformation (Fig. 9). The total magnitude of Cenozoic shortening across the Luliang Shan is ~14 km, with 8–9 km accommodated by motion on the Luliang Shan thrust and 5–6 km accommodated by folding (Fig. 9).

*Luliang Shan detachment*. Fragmentary patches and folded low-angle contacts are exposed across the Luliang Shan and Xitie Shan. They are commonly associated with mylonitic shear zones and exhibit both lower-over-higher-grade (western Luliang Shan) and higher-over-lower-grade (eastern Luliang Shan and southern Xitie Shan) relationships. Taken at face value, these contacts in their present orientation may be interpreted as either thrusts or normal faults. However, our detailed field mapping and kinematic analyses suggest that the discontinuously exposed contacts represent a single detachment surface. In the western Luliannng Shan, the low-angle contacts dip north and place epidote/amphibolite–grade mafic schist over UHP metamorphic gneiss, with generally top-north and top-east shear in the mylonitic shear zones along the contact. To the east in the eastern Luliang Shan and southern Xitie Shan, the low-angle contacts also dip north, but place higher-grade UHP metamorphic gneisses over the lower-grade mafic schist, a relationship opposite to what is observed in the western Luliang Shan, suggesting that it may be a south-directed thrust. However, closer examination of the fault-zone kinematics indicates that the fault has a top-north sense of shear (i.e., normal slip in the present orientation of the fault). These seemingly contradictory observations may be explained by the presence of a single tectonic contact, which has a generally top-north/top-east sense of shear and has been isoclinally folded (Fig. 10). The above interpretation is supported by the observation that the contact between the UHP gneisses and low-grade mafic schist is folded at various scales (a few km to tens of meters). Specifically, we observe the contact to be folded either broadly coaxial with Cenozoic folds or isoclinally defined by the folding of gneissic foliation (Figs. 8A and 9). These observations suggest that the low-angle contact we observed experienced two phases of folding: early folding under a temperature condition of >~300°C, inasmuch as quartz grains are deformed plastically, expressed by the development of a mineral stretching lineation (Hirth and Tullis, 1992), and later folding at shallow crustal conditions associated with Cenozoic shortening. The lower age bound of the later ductile folding event is defined by the age of UHP metamorphism at 488–495 Ma (Menold et al., 2003b), and the age of gneiss foliation in the UHP rocks predates ~450 Ma, as it is cut by an undeformed granite of this age (C. Menold, unpubl. data). We refer to the tectonic contact juxtaposing eclogite-bearing gneisses against the low-grade schist and metagraywacke in the Luliang Shan and Xitie Shan area as the Luliang Shan detachment.

Interpreting the Luliang Shan detachment as a single regional tectonic contact raises the question of where its extensional breakaway is located. In a typical North American Cordilleran–style extensional detachment fault system, the ductile portion of the detachment shear zone must be linked with brittle extensional faults in the hanging wall and an extensional breakaway at the surface (e.g., Lister and Davis, 1989; Yin, 2002, 2004, 2006). These types of structures do not exist above the Luliang Shan detachment where we mapped. One may argue that the breakaway and hanging-wall extensional structures are presently buried below the Cenozoic Qaidam basin. However, the continuous exposure of bedrock geology along the western and eastern ends of the Qaidam basin allows us to test this possibility; our field observations along the two outcrop strips across the basin do not support the presence of any early Paleozoic extensional structures.

*Ductile shear zones*. Ductile shear zones are present along the Luliang Shan detachment in the quartzofeldspathic gneisses below and mafic schist above. The trend of the stretching lineation in the detachment zone varies considerably, from a nearly N-S to E-W orientation. This variation could either reflect their original attitudes or later structural modification involving significant rotation about vertical axes. We prefer to interpret the variable trends as primary features because the changes in

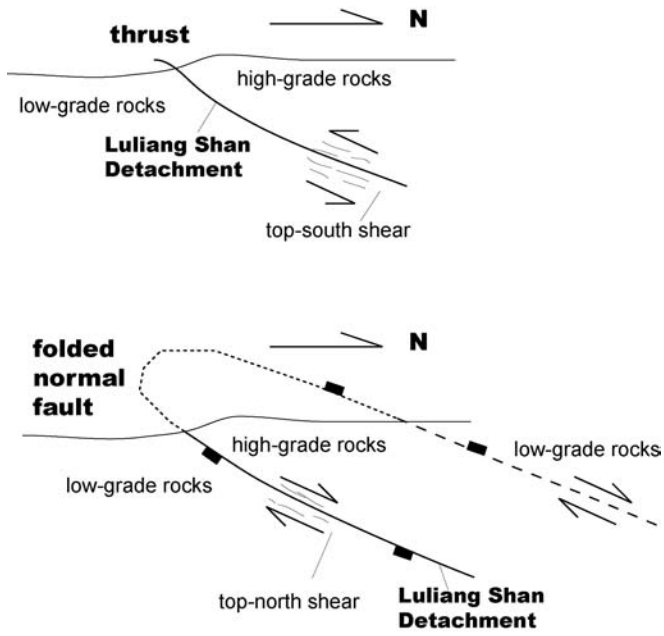


FIG. 10. Two contrasting models for the relationship between the fault orientation and fault kinematics. A. A north-dipping thrust with top-south sense of shear. B. An isoclinally folded top-north detachment fault, which exhibits a higher-grade-over-lower grade relationship, but with a top-north sense of shear.

lineation trends even occur along fault segments with relatively uniform geometry, such as along the northern edge of the western Luliang Shan (Fig. 9).

In addition to ductile shear zones directly against the Luliang Shan detachment, internal deformation of the Luliang Shan UHP metamorphic rocks is expressed by refolding of a large eclogite block in the central part of the range (Fig. 8B). Smaller eclogite blocks are present as long tails at the termination of the fold limbs, suggesting significant stretching that may be responsible for producing boudinaged eclogite blocks.

Ductile shear zones are also well developed in the Dakendaban gneiss and along the margins of the early Paleozoic plutons (Fig. 7). We observed discrete left-slip shear zones in several places in Ordovician granites. Minor top-north shear zones are also present in metagraywackes of the Dakendaban Group. All ductile shear zones outside the UHP terranes have limited lateral extent, and could not have accommodated significant strain. The age of the ductile deformation is locally constrained by its relationship to dated plutons. For example, a 442 Ma granite in the hanging wall of the Daqaidam thrust is deformed by left-slip shearing. This relationship indicates strike-slip faulting to have occurred at ~442 Ma or after.

### *P-T-t paths*

*P-T conditions.* The existing P-T data from the North Qaidam UHP metamorphic belt are summarized in Figure 11 (Yang et al. 2000, 2001; Menold et al. 2003a; Song et al. 2003, 2005, 2006; Zhang et al. 2005). Yang et al. (1994) first reported the presence of garnet peridotite in high-grade gneiss in the Luliang Shan area. This was followed by the discovery of eclogite in the same high-grade gneiss (Yang et al., 1998). The garnet peridotite contains diamond and was once under an equilibrium condition of P = 5.0–6.5 GPa and T = 960–1040°C (Song et al., 2006). Li et al. (1999) reported the discovery of coesite in eclogite blocks in the Luliang Shan, which suggests that the rocks experienced ultra-high-pressure metamorphic conditions. This result is consistent with later work by Menold et al. (2003a), who demonstrated that the Luliang Shan eclogite blocks experienced a peak pressure of 25 kbar and temperature of 625–650°C. The retrograde assemblage of the Luliang Shan eclogite was developed at pressures of 8–11 kbar and temperatures of

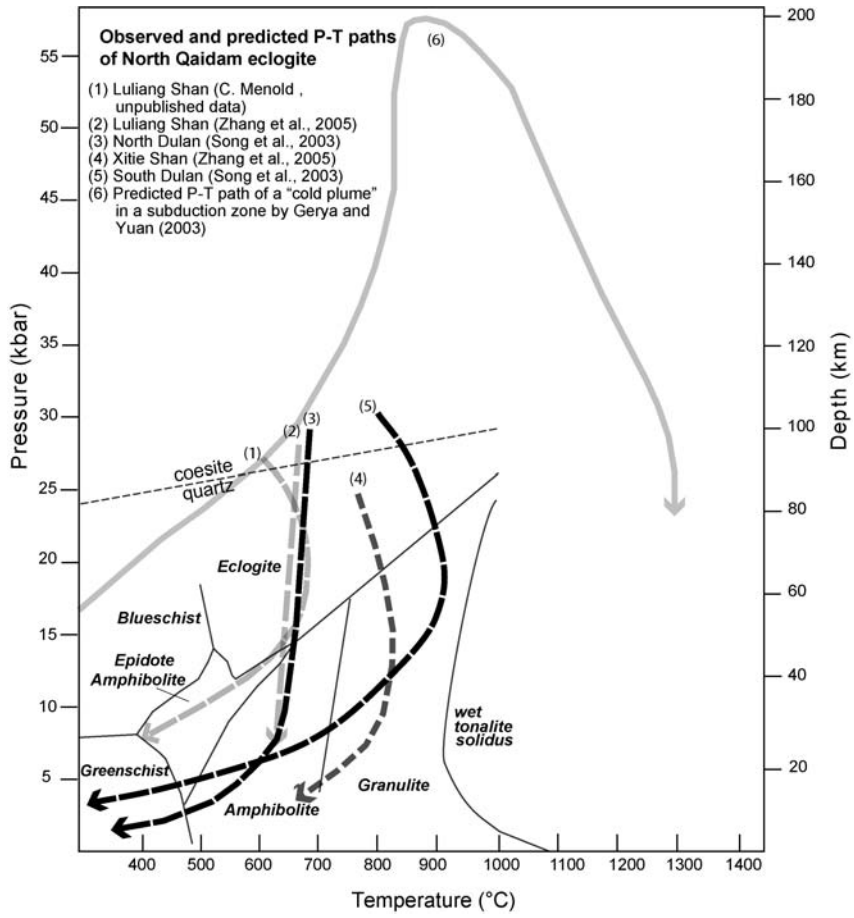


FIG. 11. P-T paths of UHP metamorphic rocks in the North Qaidam area, compiled from Yang et al. (2001), Zhang et al. (2005), Song et al. (2003, 2005, 2006), and C. Menold and C. Manning (unpubl. data). The predicted P-T path for a rising cold diapir by Gerya and Yuan (2003) is also shown.

450–520ºC (Menold et al., 2003a; Zhang et al., 2005). The P-T data of Menold et al. (2003a) and Zhang et al. (2005) also suggest a decompression path from 26 kbar and 625ºC to 6 kbar and 480ºC, with temperature either maintaining constant or increasing slightly after reaching the peak pressure (Fig. 11). The gneiss and retrograde mineral assemblage of Luliang eclogite blocks indicate stability in the epidote-amphibolite field, corresponding to depths of ~20–25 km (Menold et al., 2003a). Similar P-T paths with slightly higher temperature are also obtained in the Xitie Shan (Song et al., 2005), but both hot and cold P-T paths are obtained from the Dulan UHP metamorphic terrane (Song et al. 2003).

*Geochronology and thermochronology.* Rare-earth-element (REE) studies indicate that the garnet peridotite in the Luliang Shan was derived from oceanic mantle. These rocks experienced early Paleozoic metamorphism (457 ± 22 Ma) (Song et al., 2006). Yang et al. (2000, 2001) obtained U-Pb SHRIMP zircon ages of 443–495 Ma for the coesite-bearing paragneiss in the Dulan area, and interpreted them to represent the age of UHP metamorphism. By examining the petrology and geochronology of eclogites, Zhang et al. (2005) reported contrasting decompression paths between the Luliang Shan and Xitie Shan eclogites: the former is rapid while the latter is slow with a long

residence time of >80 m.y. in the lower crust (Figs. 11 and 13).

U-Pb dating of metamorphic zircons from the Luliang Shan eclogite indicates that UHP metamorphism occurred at ~488–495 Ma (Menold et al., 2003b; Zhang et al., 2005). Similar studies show UHP metamorphism to have occurred at ~478–488 Ma in the Xitie Shan (Zhang et al., 2005) and at ~422–450 Ma in the Dulan region (Song et al., 2005; Mattinson et al., 2006). The above data suggest that North Qaidam UHP metamorphism was protracted, lasting for tens of million years. The eastward decrease in UHP metamorphic ages could either be related to diachronous UHP metamorphism, or to coeval exhumation and emplacement of UHP metamorphic rocks during crustal thickening. That is, if exhumation occurs during episodic emplacement of UHP metamorphic rocks in the lower crust, the older UHP rocks may have been exhumed to shallow crustal levels while the younger UHP rocks were emplaced at deeper crustal levels (Fig. 12). Also, strike-slip tectonic tilting could subsequently expose UHP metamorphic rocks with different metamorphic ages. Regardless of which mechanism is correct (diachronous UHP metamorphism vs. structural stacking), the age of North Qaidam UHP metamorphism overlaps in space and time with regional arc magmatism between 520 and 400 Ma (Cowgill et al., 2003; Gehrels et al., 2003a) (Fig. 4).

$^{40}Ar/^{39}Ar$ cooling ages of white mica indicate that UHP rocks were exhumed to the middle crust at ~465–390 Ma at the Luliang Shan and the Xitie Shan and ~400 Ma in the Dulan area (Menold et al. 2003b; Song et al., 2005; Zhang et al., 2005). Specifically, $^{40}Ar/^{39}Ar$ thermochronological analysis revealed a large variation of mica ages from 465 to 390 Ma over a distance of <10 km in the western Luliang Shan, indicating that the UHP metamorphic rocks there had stayed at mid-crustal depths over some 70 m.y. before finally being exhumed to the upper crust (C. Menold, unpubl. data). T-t paths of the North Qaidam UHP metamorphic rocks derived from the above U-Pb zircon ages and $^{40}Ar/^{39}Ar$ amphibolite, muscovite, and biotite thermochronology are summarized in Figure 13.

### *Protolith of mafic and ultramafic rocks in UHP metamorphic rocks*

The protoliths of eclogite blocks in the North Qaidam UHP metamorphic terranes could either be from mafic igneous rocks such as dike swarms emplaced along a rifted continental setting or from fragments of oceanic crust originated in island-arc settings or at mid-ocean spreading centers. Nd isotopic data from the Luliang Shan and Xitie Shan eclogites indicate that they were derived from a highly depleted mantle, with εNd ($\tau$ model = 800 Ma) values ranging from 3.05 to 9.20; the 800 Ma Nd model age is based on U-Pb zircon ages of the eclogite (Song et al., 2006). This observation suggests that the eclogites were derived either from a back-arc or mid-ocean-ridge setting, but not from a continental setting (Zindler and Hart, 1986). Rare-earth-element patterns for Dulan eclogite suggest that the protolith of the eclogite could represent mid-ocean-ridge basalt (MORB) or oceanic island basalt (OIB) (Song et al., 2003). However, the same REE pattern could also be explained by emplacement of mafic dikes into a newly rifted continental margin. The latter mechanism would have allowed mixing of continental and "oceanic-like" mafic materials before they underwent UHP metamorphism.

### *Sources of continental materials in UHP metamorphic rocks*

Several processes may have led to incorporation of continental materials into the North Qaidam UHP metamorphic rocks: (1) tectonic erosion that includes subduction of accretionary prisms (e.g., Crowell, 1981; Cloos and Shreve, 1988a, 1988b; Balance et al., 1989; von Huene and Lallemand, 1990; Vannucchi et al., 2001), fore-arc basins (Hall, 1991; Barth and Schneiderman, 1996; Saleebey, 2003), and over-riding continental crust; (2) subduction of ocean-continent transition zones with both oceanic and continental crust; and (3) subduction of a rifted continental margin (Fig. 14). The last mechanism could be lumped into the tectonic-erosion mechanism.

*Tectonic erosion*. In an evolving subduction system, such as the Late Cretaceous–early Tertiary western North America and the Cenozoic South America subduction zones, accretionary prisms containing continental detritus could be buried tectonically during oceanic subduction (e.g., Barth and Schneiderman, 1996; Vannucchi et al., 2001; Usui et al., 2003). Given the large size of the accretionary complex across the western Qilian orogen but a very narrow belt across the eastern Qilian orogen (Fig. 2), we envision that this process may have occurred in the Dulan region, where UHP metamorphism occurred in the waning stage of arc

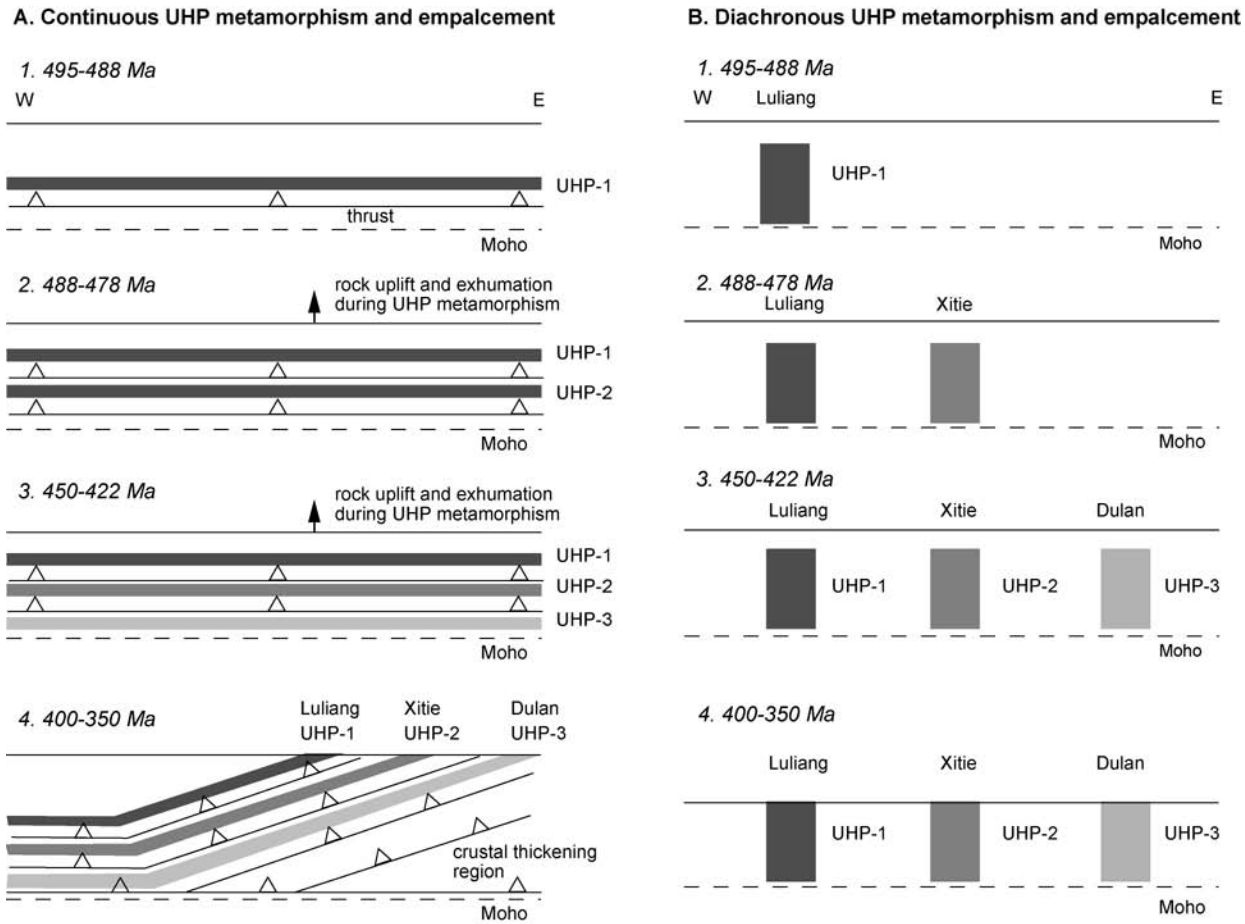


FIG. 12. Two possible mechanisms to explain the diachronous UHP metamorphic ages in North Qaidam. A. Continuous emplacement of UHP metamorphic rocks into lower crust during coeval crustal shortening and exhumation. B. Episodic emplacement of UHP metamorphic rocks along strike, with the oldest event in the west, and migrating to the east.

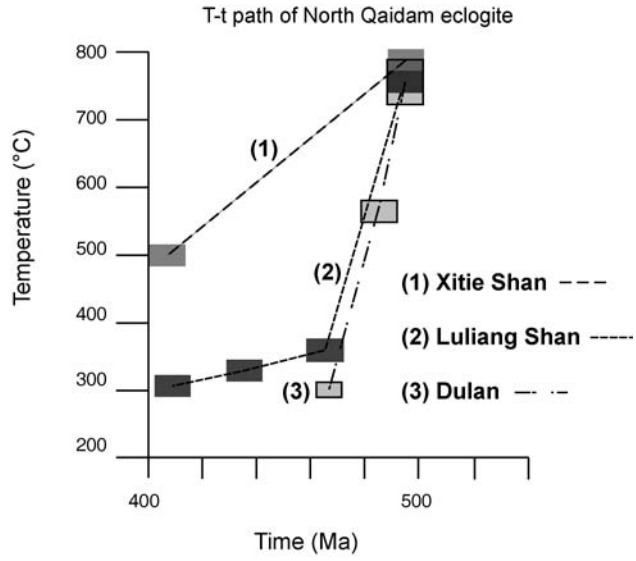


FIG. 13. T-t paths of North Qaidam UHP metamorphic rocks (see text for sources).

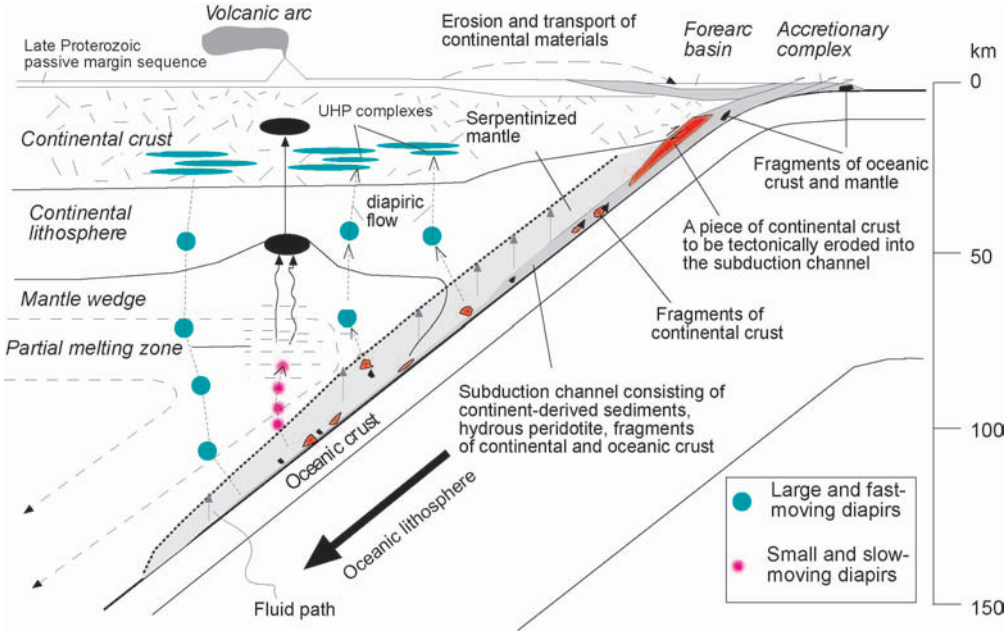


FIG. 14. Conceptual model for the coeval occurrence of arc magmatism and UHP metamorphism based on Hall and Kincaid's (2001) model. Large diapirs launching from the subduction channel rise rapidly across the mantle wedge, avoiding partial melting. In contrast, small diapirs travel slowly across the mantle wedge, allowing them to be gradually heated, leading to partial melting. Emplacement of the large diapirs into the lower crust at the base of the arc will become the UHP metamorphic terrane, while emplacement of partially melted rocks will become the arc plutons and volcanic rocks.

magmatism around 450–420 Ma (Mattinson et al., 2006), allowing a significant amount of time (>50–80 m.y.) to accumulate accretionary materials to be subducted along with the oceanic slab (e.g., Song et al., 2006) (Figs. 2 and 14A). In addition to subducting oceanic mélange complexes, the over-riding continental crust also could have been eroded tectonically and carried to mantle depths by the oceanic slab.

*Subduction of continent-ocean transition zone*. We note that the oldest age of UHP metamorphism is close to the oldest age of regional arc magmatism across the southern Qilian orogen, at ~490–480 Ma (Fig. 4). This relationship implies that the development of North Qaidam UHP metamorphism may have occurred at the onset of oceanic subduction. One possible way of incorporating both continental and oceanic materials into the UHP metamorphic rocks is by subducting the continent-ocean transition zone, which may include individual fragments of continental and oceanic crust or continental fragments with mafic dike swarms inherited from earlier rifting. This hypothesis may apply to the Luliang Shan and Xitie Shan areas, where UHP metamorphism appears to have taken place over a few million years during the earliest stage of arc magmatism. Two lines of evidence support this argument. First, the transition zone between the continental and oceanic crust along a continental margin can be highly irregular (Whitmarsh et al., 2001). Second, numerical simulations by Regennauer-Lieb et al. (2001) indicate that initiation of oceanic subduction most likely occurs along the oceanic-continental crust transition where a large amount of sediments accumulated; the latter produces flexural bending and stress concentration, causing the plate to break and sink. These two conditions require that initial oceanic subduction may carry a mixture of continental and oceanic crustal materials to depth under UHP metamorphic conditions, which could subsequently return to the over-riding plate via diapiric flows (Fig. 14B) (also see discussion below).

## Emplacement Mechanism of UHP Metamorphic Rocks

The major observations derived from the North Qaidam UHP metamorphic belt may be summarized below.

1. UHP metamorphism in the North Qaidam region occurred between 495 and 420 Ma, with a progressively eastward-younging metamorphic age. Its occurrence overlaps in space and time with regional arc magmatism across the Qilian orogen (Figs. 3 and 4).

2. Exhumation of the UHP rocks was rapid, bringing the rocks from a depth of >90 km to lower and middle crustal levels (~30 km) in less than 10 million years (Fig. 13).

3. Cooling of the UHP rocks occurred slowly over tens of million years at lower and middle crustal depths (Fig. 13).

4. The tectonic contact between UHP metamorphic rocks and lower-grade metamorphic rocks, as represented by the Luliang Shan detachment, has been modified by early Paleozoic ductile folding and later by Cenozoic folding.

5. The kinematics of the Luliang Shan detachment are complex, with stretching lineation trends in variable directions. This variability represents the original transport direction when the UHP metamorphic rocks were emplaced into the lower crustal depths.

6. Refolded eclogite sheets and widespread eclogite boudins require the UHP metamorphic terranes to have been intensely deformed internally via complex ductile flow before exhumation to the upper crust.

7. The protolith of the UHP metamorphic rocks is a mixture of continental crust and mafic materials.

8. The North Qaidam UHP metamorphic rocks may have been emplaced in an oceanic mélange in the southern Qilian orogen as represented by the Ordovician metagraywacke and widely scattered ultramafic rocks.

9. No early Paleozoic extensional breakaway system can be identified across the southern Qilian orogen except for the Luliang Shan detachment. That is, the Luliang Shan detachment is a tectonic contact accommodating deformation between the UHP metamorphic rocks and lower-grade mafic schist.

In order to determine the emplacement mechanism of the North Qaidam UHP metamorphic rocks, we evaluate the major existing tectonic models for UHP metamorphism in the context of the observations above (Fig 1; Table 1). First, we can rule out the continent-continent collision model and the associated wedge-extrusion process because this model predicts UHP metamorphism to postdate arc magmatism, and involves rapid exhumation of wedge-shaped continental crust between a thrust below and a normal fault immediately after the initial collision. None of these predictions match our

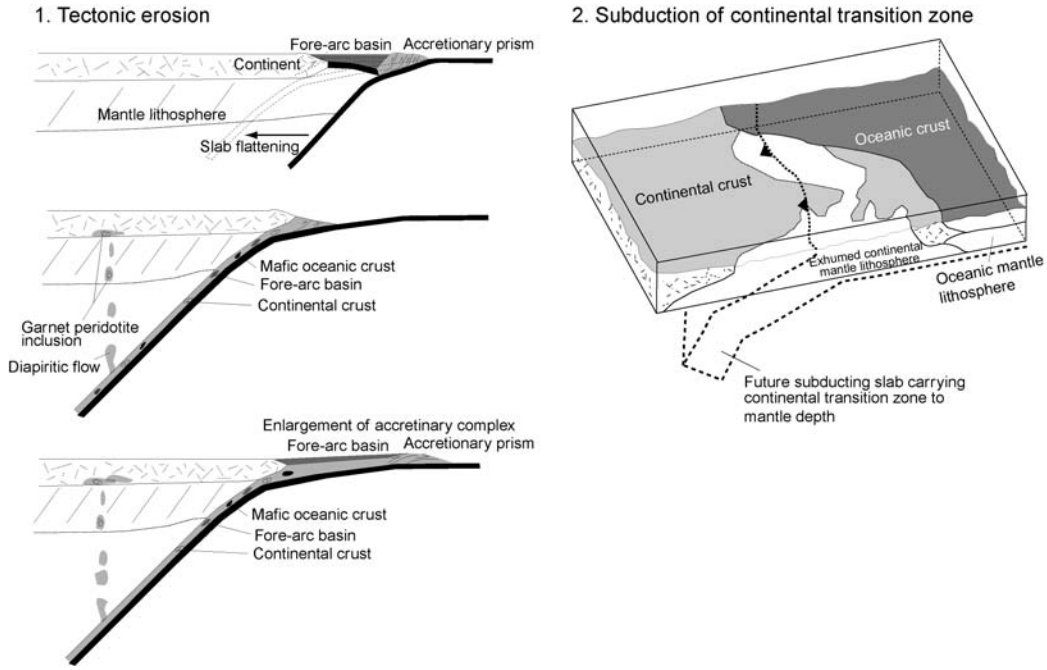


FIG. 15. Possible mechanisms for incorporating continental and mafic materials into oceanic subduction channels. A. Tectonic erosion including incorporating materials from accretionary prisms, fore-arc basins, and rifted continental margin in overriding plate. B. Subduction of ocean-continent transition zone that has an irregular contact.

observations from the North Qaidam UHP metamorphic belt, as discussed above. Second, we can also eliminate the Cloos-type corner-flow model, either during oceanic or continental subduction as an unlikely mechanism (Cloos, 1982; Mancktelow, 1995). This is because it predicts exhumation of UHP metamorphic rocks from a depth of >70–90 km to a near-surface condition in a single and rapid exhumation process at a plate tectonic rate. That is, the UHP metamorphic rocks should have traveled from a depth of >70–90 km to the surface in less than a few million years, which is inconsistent with our observed long resident time of >50–70 million years in the lower crust. Finally, we rule out the model advocating diapiric flow during continental subduction after ocean closure across the Qilian orogen, because it is inconsistent with our observation that UHP metamorphism occurred during rather than after regional arc magmatism. Eliminating the above models, the observations listed above lead us to suggest that the prograde metamorphism of the North Qaidam UHP rocks may have been related to oceanic subduction. Specifically, this process may have carried a mixture of continental and oceanic materials along a subduction channel to a depth >70–90 km, with the subducted materials later exhumed via diapiric flow to lower and middle crustal depths where they reached neutral buoyancy and became trapped (Fig. 15).

## Thermomechanical Model for UHP Metamorphism via Diapiric Flow

We presented our diapiric flow model for UHP metamorphism in 2001 (Yin et al., 2001) when we had little field and P-T-t data to constrain North Qaidam UHP metamorphism. With tighter constraints on protolith, regional tectonic history, and P-T-t paths from several recent studies on the North Qaidam metamorphic rocks, we are now able to address whether diapiric flow is mechanically feasible and what P-T-t paths are predicted during this process.

### *Mechanism of synchronous UHP metamorphism and arc magmatism*

A potential obstacle to diapiric flow of subducted crustal materials would be high mechanical strength

of the mantle wedge that would cause it to act as a rigid body. This in turn would confine subducted materials in a channel (Cloos, 1982; Shreve and Cloos, 1986; Mancktelow, 1995). This is certainly the case in the upper 20–30 km of a subduction zone where temperature is low and rock strength is high. However, as the mélange materials are subducted deeper, the strength of mantle rock decreases due to both thermal and hydraulic softening effects (Hirth and Kohlstedt, 1996; Mei and Kohlstedt, 2000). If the wall rock is weak enough, the buoyancy of the subducted mélange materials may overcome the resistance from the overlying mantle (Fig. 15).

Hall and Kincaid (2001) explored the mechanics of diapirs traveling through a mantle wedge using analogue experiments. They showed that the ascending style of a buoyant fluid is a function of a dimensionless number

$$B_n = \frac{\Delta\rho g Q}{\mu_0 U_0^2} \quad (1)$$

where $\Delta\rho$ is the difference between the buoyant fluid (= mélange materials) and the matrix (= mantle), $g$ is the gravitational acceleration, $Q$ is the volumetric flux of the buoyant fluid from the subduction zone (= flux of subducted materials), $\mu_o$ is the effective viscosity of the mantle, and $U_o$ is the subduction velocity. At low values of $B_n$ ($\sim 10^{-4}$ to $10^{-5}$) (i.e., fast convergence or low sediment flux), the buoyant fluid forms diapirs of uniform radius and ascend at regular time intervals with a transient time of 3–6 m.y. At intermediate values of $B_n$ ($\sim 10^{-4}$), diapirs form at irregular time intervals with a wide range of sizes. The larger diapirs ascend quickly with a transient time of 0.7 to 3 million years across the mantle wedge and do not partially melt. In contrast, smaller diapirs rise slowly and experience partial melting. Finally, high values of $B_n$ ($\sim 10^{-3}$ to $10^{-4}$) can lead to a network-flow regime in which several ascending diapir paths merge into a single continuous conduit with a transient time of only $10^4$ to $10^6$ years. The most important result of the above experiments with regard to UHP metamorphism is that only under a small range of parameterization (i.e., with intermediate $B_n$ values) can arc magmatism and isothermal decompression of UHP metamorphic rocks occur.

Although Hall and Kincaid's (2001) work provides a useful conceptual framework for UHP metamorphism during oceanic subduction, applying this model directly to explain the observed P-T-t paths is problematic. First, the model assumes isoviscous and isothermal conditions for diapir transport. Therefore, the effect of temperature-dependent mantle rheology cannot be evaluated. Second, the analogue-model fluids are Newtonian, which is not appropriate for the power-law rheology of the mantle wedge. Third, the ascent velocity of diapirs in their thermal calculations is assumed to be uniform throughout their travel paths. As we show below, this is unlikely in a mantle wedge with a temperature-dependent rheology. Fourth, the thermal calculations for the rising diapirs by Hall and Kincaid (2001) were based on the assumption that the Peclet number is high ($Pe >> 1$), allowing them to use the classic formulation of Marsh and Kantha (1978); this approach ignores the effect of conductive cooling when the diapir transport velocity is low.

To overcome the limitation of the Hall and Kincaid (2001) approach, Gerya and Yuan (2003) developed a fully coupled thermal-dynamic model to track the thermal and fluid-flow evolution of a subduction zone. They paid particular attention to track P-T-t paths of cold plumes similar to the diapirs modeled in Hall and Kincard's analogue models using a 2-D numerical code. Their model predicts that diapirs launch at a depth of ~200 km and experience a peak temperature exceeding 1200°C. This predicted temperature far exceeds the highest observed temperature from the North Qaidam UHP metamorphic belt (Fig. 11). Although the model by Gerya and Yuan (2003) considers realistic rheology and possible phase changes during diapiric ascent, its complex parameterization makes tracking the physics of diapir transport difficult.

### *Thermomechanical model*

To overcome the limitations in the approaches of Hall and Kincaid (2001) and Gerya and Yuan (2003), we developed a simple scheme to calculate P-T-t paths of rising diapirs across mantle wedges. In our approach, we use a series of simple analytical solutions derived from basic diapir mechanics and integrate them with known thermal models for a subduction zone under various plate-convergent conditions. This approach allows us to evaluate the thermal and mechanical processes of individual diapir ascent and to calculate P-T-t paths that can be compared directly against observed P-T data.

*Ascent velocity.* First, we use the Hadamard-Rybczynski equation to calculate ascent velocity $V$ of a Newtonian-fluid sphere traveling through a

power-law fluid (Weinberg and Podladchikov, 1994):

$$V = \frac{1}{3}\frac{\Delta\rho g r^2}{\mu_{eff}}\left(\frac{1}{X_{sol}}\frac{G\mu_{eff}+\mu_{sph}}{GM\mu_{eff}+1.5\mu_{sph}}\right)^n \quad (2)$$

where $\mu_{eff}$ is the effective viscosity of the ambient power fluid, $\mu_{sph}$ is the Newtonian viscosity of the sphere, $r$ is the radius of the sphere, and $\Delta\rho$ density difference between the sphere and the ambient power-law fluid. Parameter $n$ is a constant in a power law that has the following form:

$$\dot{\varepsilon} = A\sigma^n \exp(-E/RT) \quad (3)$$

where $\dot{\varepsilon}$ is strain rate, $\sigma$ is stress, $A$ is a material constant, $E$ is activation energy, $R$ is the gas constant, and $T$ is temperature. Constants $G$, $X_{sol}$, and $M$ in (2) are material properties related to $n$ (Weinberg and Podladchikov, 1994). The effective viscosity of the power-law fluid $\mu_{eff}$ is defined by (Weinberg and Podladchikov, 1994) as:

$$\mu_{eff} = \mu_0 e^{E/RT} \quad (4)$$

where

$$\mu_0 = \frac{6^{n-1}}{3^{(n+1)/2}A(\Delta\rho g r)^{n-1}} \quad (5)$$

The above relationship states that the strength of the mantle wedge through which a diapir passes is a function of temperature ($T$), density contrast ($\Delta\rho$), diapir size ($r$), and activation energy ($E$). An increase in the first three parameters ($T$, $\Delta\rho$, $r$) would decrease the mantle viscosity while an increase in $E$ would increase the mantle viscosity (Fig. 16C).

Inserting (4) into (2), we obtain the velocity as a function of temperature as:

$$V = V_0 e^{-E/RT} \quad (6)$$

where

$$V_0 = \frac{2}{9^n}\frac{(\Delta\rho g r)}{\mu_0 X^n} \quad (7)$$

The above relationship indicates that the transport velocity of a diapir increases with density contrast ($\Delta\rho$) and diapir size ($r$) but decreases with activation energy ($E$). In our calculations below, we assume that $\Delta\rho$ is a constant equal to 500 kg/m$^3$ throughout the history of diapir ascent.

*Size of ascending diapirs*. The size of diapirs, as measured by their diameters $d = 2r$ and initiated by the Rayleigh-Taylor instability, can be estimated by the following relationship (Marsh, 1979):

$$d = h_2\left(\frac{\mu_1}{\mu_2}\right)^{1/4} \quad (8)$$

where $h_2$ is the thickness of a subduction channel, $\mu_2$ is the viscosity of the mélange materials in the channel, and $\mu 1$ is the viscosity of the overlying mantle. This relationship suggests that a weaker and thicker mélange channel produces larger diapirs. The thickness of a subduction channel is typically a few hundreds of meters thick (e.g., Ye et al., 1996), and the viscosity for a sedimentary mélange and the mantle wedge above a subducting slab is about $10^{10}$ Pa s and $10^{18}$ Pa s, respectively (Hall and Kincaid, 2001). Using the above viscosities and assuming $h_2$ varying between 200 and 400 m, the diameter of the corresponding diapir $d$ would range between 20 and 40 km. Below we use $r$ = 10 km throughout our calculations.

*Geotherms*. Because the ascent velocity in (6) is temperature-dependent, we need to define the geotherm along the ascent path of a diapir, which requires the knowledge of thermal structures in a subduction zone. There are two approaches in simulating the thermal structure of a subduction zone: one by assuming the mantle to flow as an isoviscous Newtonian fluid whereas the other assumes mantle to follow a temperature-dependent power law (Peacock and Wang, 1999; cf., van Keken et al., 2002). The key difference between the two models is that the power-law model predicts a few hundreds of degrees higher temperature within the mantle wedge and at the subducting slab surface (van Keken et al., 2002). That is, the thermal structures derived from isoviscous conditions possibly represent a lower temperature bound of a realistic subduction zone.

In our calculations, we choose two geotherms ranging in depth from 100 to 0 km from the thermal models of Peacock and Wang (1999) (Fig. 16). A cold geotherm was constructed from their model for a fast (91 mm/year) and old subduction zone (130 Ma), whereas a warm geotherm was constructed from a slow (45 mm/year) and younger (15 Ma) subduction zone. We also use two other hypothetical geotherms in our calculations of P-T paths (Fig. 16).

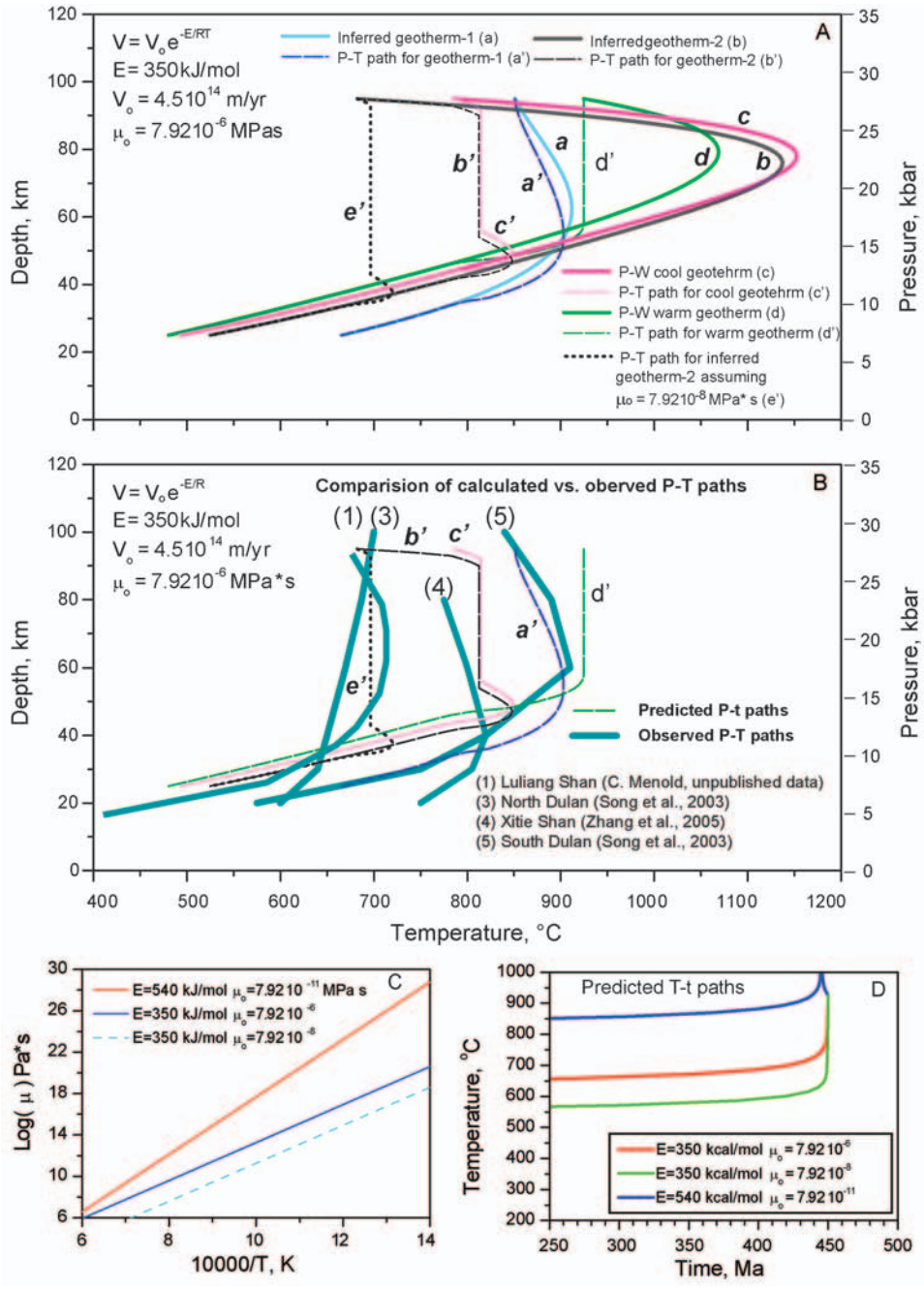


FIG. 16. A. Geotherms and predicted P-T paths. Paths labeled P-W are from Peacock and Wang (1999). B. Comparison of predicted vs. observed P-T paths from the North Qaidam region. C. Relationship between effective viscosity of mantle wedge and temperature. D. Predicted T-t paths as a function of activation energy *E* for olivine aggregates.

*Rheology of the mantle wedge*. In the olivine flow law, parameters $n$ and $A$ are relatively well constrained (Kirby, 1983), and we assume $n = 3.5$ and $A = 6.34 \times 10^4$ MPa$^{-n}$ s$^{-1}$ in our calculation. The great uncertainty comes from the estimate of olivine activation energy that can vary from ~330 kJ/mol to ~530 kJ/mol for dry olivine (Kirby, 1983). When the role of water and melts are considered, the effective viscosity of the upper mantle can be reduced by two to three orders of magnitude (Hirth and Kohlstedt, 1996; Mei and Kohlstedt, 2000).

*Thermal evolution of rising diapirs*. Once a geotherm and the rheology of the mantle wedge are selected, we can derive the ascent velocity as a function of depth and compute temperature history of the rising diapir (Fig. 16). Our thermal calculations consider the following two competing situations. First, we consider thermal diffusion of a diapir as it passes through the mantle when the ascent velocity is slow. This is the situation when thermal diffusion dominates and the Peclet number is small. The Peclet number for a moving sphere is defined as

$$Pe = \frac{Vr}{K} \tag{9}$$

where $V$ is the ascending velocity, $r$ the radius of the sphere, and $K$ the thermal diffusivity. For Pe <<1, we can calculate the average temperature of a moving diapir along a geotherm from the relationship below (Carslaw and Jaeger, 1959):

$$\Delta T = (T_m - T)\left(1 - \frac{6}{\pi}\sum\frac{1}{n^2}e^{-n^2\pi^2\frac{\Delta z}{rPe}}\right) \tag{10}$$

where $\Delta T$ is an incremental temperature change of the diapir from a position at $z_i$ to the next position at $z_{i+1}$ when it travels across a vertical distance of $\Delta z = z_{i+1} - z_i$. $T_m$ is the ambient temperature representing the geotherm, and $T$ is the average temperature of the diapir, which is a function of depth $z$.

For Peclet number $Pe$ >>1, heat flux $Q_{out}$ across a diapir equals its change in internal energy ($\Delta E_{int}$) (Marsh and Kantha, 1978):

$$Q_{out} = \Delta E_{int}. \tag{11}$$

This leads to the following relationship (Marsh and Kantha, 1978):

$$T(t) = Je^{-Jt}\int e^{Jt}T_m(t)dt \tag{12}$$

where $J = 3NuK/r^2$, with $Nu$ as the Nusselt number for an ascending diapir that is defined by:

$$Nu = \frac{2}{\sqrt{6\pi}}Pe^{1/2}\left(\frac{\mu_{eff}}{\mu_{eff} + \mu_{sph}}\right) \tag{13}$$

$T(t)$ in (12) is the average temperature of the ascending diapir, and $T_m(t)$ is the ambient temperature (i.e., the geotherm) in the mantle wedge, through which the diapir passes.

*Model results*

In order to simulate our observed P-T and T-t paths from the North Qaidam UHP metamorphic belt, we adopted four different geotherms from a depth of 100 km on the top of a subducting slab to Earth's surface: (1) a hot geotherm from Peacock and Wang (1999) for a young oceanic lithosphere subducting at a slow rate (P-W warm geotherm in Figure 16A); (2) a cool geotherm from Peacock and Wang (1999) for an old oceanic crust subducting at a fast rate; (3) a hypothetical geotherm with a slab surface temperature of 700°C at the depth of 100 km (inferred geotherm-1 in Fig. 16A); and (4) a hypothetical geotherm with a temperature of 850°C at the depth of 100 km (inferred geotherm-2 in Fig. 16A). For case (3), the temperature distribution is essentially the same as the P-W cool geotherm except that we lower the slab surface temperature by about 100°C. This may simulate a situation in which diapirs were launched within the cooler subducted mélange channel above the slab surface.

With all other conditions equal, we found that the calculated P-T paths are very sensitive to the geotherm and in particular to the temperature at which a diapir was launched. For the P-W warm geotherm (curve *d* in Fig. 16A), the corresponding P-T path of the diapir with $r = 10$ km and $E = 350$ kJ/mol (curve *d'* in Fig. 16A) initially has a nearly isothermal trajectory from ~100 km to ~42 km and then follows the geotherm to cool gradually. This P-T path is rather typical for those under different geotherms and its physics can be easily understood. For the isothermal part of the P-T path, the thermally activated olivine flow law allows rapid passage of the diapir through the hottest part of the mantle wedge. Because of the high ascent velocity and thus high Peclet number, the effect of thermal diffusion of the rising diapir as a result of ambient heating is negligible. That is, the diapir behaves like an ice ball traveling rapidly through a hot water tank without becoming molten. When the diapir reaches

the cooler upper part of the upper mantle wedge or lower crust, its ascending speed slows and thermal diffusion takes over. This allows the diapir to reach thermal equilibrium with its surrounding temperature as represented by the geotherm. As shown in Figure 16B, the P-W warm geotherm provides an upper bound for our observed P-T paths from the North Qaidam region.

Using the P-W cool geotherm, our calculation predicts nearly isothermal decompression from a depth of 100 km to about 50 km for the rising diapir ($r$ = 10 km and $E$ = 350 kJ/mol; curve *c'* in Fig. 16A). The temperature of the diapir increases slightly (~50°C) from 50 km to 40 km due to adiabatic heating and then follows the geotherm to a depth of ~20 km. This calculated P-T path broadly resembles the observed P-T path of the Xitie Shan eclogite (compare curve [4] with curve *c'* in Fig. 16B; Zhang et al., 2005). Under the same condition as in the two previous cases ($r$ = 10 km and $E$ = 350 kJ/mol), we find that a hotter slab surface temperature and a cooler interior temperature of the mantle wedge would allow us to simulate the observed P-T path from the southern Dulan region (compare curve [5] with curve *a'* in Fig. 16B).

Although the geotherms from the Peacock and Wang (1999) model allow us to simulate well the hotter P-T paths observed from the North Qaidam UHP metamorphic belt, they do not generate the cooler P-T paths such as those observed in the Luliang Shan and the northern Dulan region (Fig. 16B). To address this question, we first lowered the slab surface temperature at which the diapir is launched from the P-W cool geotherm from 800°C to 700°C (curve *b* in Fig. 16A). Under this condition, the diapir travels slowly and its thermal state is closely resembled by the geotherm, as thermal diffusion dominates. The diapir has to reach a temperature of ~800°C to be able to travel isothermally across the mantle wedge (curve *b'*, Fig. 16A). This relationship implies that the buoyancy was not large enough to overcome the viscous resistance of the mantle wedge to have a rapid launch. We are able to simulate the observed cooler P-T paths from North Qaidam by lowering $\mu_0$ for two orders of magnitude (curve *e'* in Figs. 16A and 16B). An identical result can be obtained by lowering $e^{E/RT}$ in (4) by two orders of magnitude. We consider the latter case more likely because water can lower the effective viscosity of olivine by two to there orders of magnitude (Hirth and Kohlstedt, 1996).

One of the hallmarks of UHP metamorphic rocks in the North Qaidam region is their rapid exhumation from upper mantle depths to the lower crust (90–70 km to ~40–30 km) (Fig. 13). In our calculations, we found that a low effective viscosity of the mantle wedge, particular in the low range as envisioned by Hirth and Kohlstedt (1996), allows rapid exhumation of UHP metamorphic rocks from a depth of 100 km and a temperature of 700–850°C to ~550°C within a few million years (Fig. 16D). The weaker the mantle rheology, the shallower the structural level to which a diapir can be emplaced.

## Discussion

### *Implications of the diapiric flow model*

The results of our diapiric flow model and their match to the observed P-T and T-t paths from North Qaidam imply that the North Qaidam UHP metamorphic rocks were produced under diverse thermal regimes and mechanical conditions during oceanic subduction. This result is in contrast to the predicted P-T paths from the wedge-extrusion model, which requires the entire exhumed continental slab to share similar P-T paths (e.g., Ernst and Peacock, 1996).

Our diapir model is thermally opposite to that of hot Stokes models of Marsh (1982) and Mahon et al. (1988). In their models, the heat diffused from a rising diapir softens its wall rocks and thus allows the diapir to ascend upward while it cools. In contrast, our cold diapirs going through the mantle wedge may potentially become hotter, depending on the assumed geotherms and the rheology of the mantle (Fig. 16). Qualitatively, preservation of UHP mineral assemblages requires either that the diapirs are sufficiently large or that the mantle wedge is weak enough for the diapirs to travel rapidly through the mantle wedge. This allows the diapirs to remain cold from their initial conditions at ~700–750°C even though they travel through regions with temperatures as high as 1200°C. Our model also implies the following conditions to favor the occurrence of diapiric flow during oceanic subduction: (1) young oceanic crust with a warm geotherm; (2) a subduction zone in its early stage of development; and (3) a delicate balance between the subduction rate and the flux of subducted sediments (i.e., the optimal $B_n$ value that allows diapiric flow as shown by Hall and Kincaid, 2001).

The emplacement depth of a diapir is controlled by neutral buoyancy, which is most likely located at

the base of the continental crust, where the density contrast between the diapir and its surrounding rocks disappears. This mechanism, as implied in our model, predicts that subducted oceanic and continental materials could have been extensively underplated and ponded at the base of an arc (Fig. 14). A test for this prediction is to examine xenoliths included in younger volcanic rocks that were erupted through major magmatic arcs. A good example of such test may be illustrated by the occurrence of coesite- and lawsonite-bearing eclogite xenoliths from the Colorado Plateau of the western United States (e.g., Usui et al., 2003). These authors show that the xenoliths were formed in a low-temperature and high-pressure environment within subducted oceanic lithosphere; they were later brought up to the surface by mid-Tertiary volcanic eruption. A similar case has been made for the Cretaceous Sierra Nevada batholith, where Cenozoic volcanic eruption carried eclogite-facies xenoliths to the surface (Ducea, 2001). Although the occurrence of the xenoliths was explained by delamination of a thick mafic lower crust beneath the Sierra arc (Ducea and Saleeby, 1996, 1998), an alternative is subduction of oceanic and continental materials into the mantle, with subsequent exhumation via diapiric flow across the mantle wedge during subduction of the Farallon plate below North America. The process of subducting a large amount of continentally derived sediments can be confidently established along the western margin of the North American Cordillera, as expressed by the exposure of Orocopia-Pelona-Rand schist in California (e.g., Crowell, 1981; Jacobson et al., 1996; Yin, 2002); this process may extend deeper than previously thought into the upper mantle, as demonstrated by the above two cases.

We note that in both the Kokchetav UHP metamorphic complex of northern Kazakhstan (e.g., Kaneko et al., 2000) and the Sulawesi subduction complex containing coesite-bearing eclogite in eastern Indonesia (Parkinson et al., 1998), metamorphism under the UHP condition occurred synchronously with regional arc magmatism (see Zonenshain et al., 1990 for the geologic history of the Kokchetav region and Wakita, 2000, for the geology of the Sulawesi region). Coeval arc magmatism and UHP metamorphism could also be inferred for the occurrence of D'Entrecasteaux Island eclogites in eastern Papua New Guinea (Baldwin et al., 2004). We suggest that the development of UHP metamorphism and subsequent exhumation of the UHP metamorphic rocks in these regions were related to diapiric flows during oceanic subduction.

Although our thermomechanical model was used to calculate P-T and T-t paths for diapiric flows during oceanic subduction, the general principles and the results can be applied to continental subduction and possibly related diapiric flows. A case to be made is the presence of near-UHP xenoliths in Miocene volcanic rocks in the Pamirs at the western end of the Himalayan-Tibetan orogen (Searle et al., 2001; Hacker et al., 2005). The protolith of the xenolith was derived from the southern margin of Asia that may have been tectonically eroded and subsequently carried down to depths of >70 km by the subducting Indian continent. The position of the xenoliths in the overriding Asian plate in the Pamirs suggests that they were transported across the mantle wedge, possibly via diapiric flow to the lower or upper crust of the overriding plate, and were finally carried to Earth's surface by volcanic eruption.

### *Classification of UHP metamorphism by tectonic settings and emplacement mechanisms*

Many geologic features can be generated by diverse mechanisms. For example, folds may develop by buckling, bending, and propagation of blind thrust, among many other mechanisms. Similarly, we suggest that UHP metamorphism could also occur under different mechanisms associated with different tectonic processes and tectonic settings. The slab breakoff and wedge-extrusion models appear to explain the occurrence of UHP metamorphism in the Himalayan and Qinglin-Dabie orogens (Ernst and Liou, 1995; O'Brien et al., 2001; Kohn and Parkinson, 2002). In contrast, geologic observations from the Variscan French Massif Central favors channel flow within accretionary wedge during oceanic subduction (Lardeaux et al., 2001). As mentioned above, our diapiric flow model may explain the occurrence of North Qaidam UHP metamorphism in western China, the development of the Kokchetav UHP metamorphic complex in northern Kazakhstan (e.g., Kaneko et al., 2000), and the formation of the Sulawesi UHP subduction complex in eastern Indonesia (e.g., Wakita, 2000). Finally, diapiric flow during continental subduction may explain the occurrence of a near-UHP metamorphic condition below the Pamirs in the overriding plate of a continent-continent collision zone (Hacker et al., 2005).

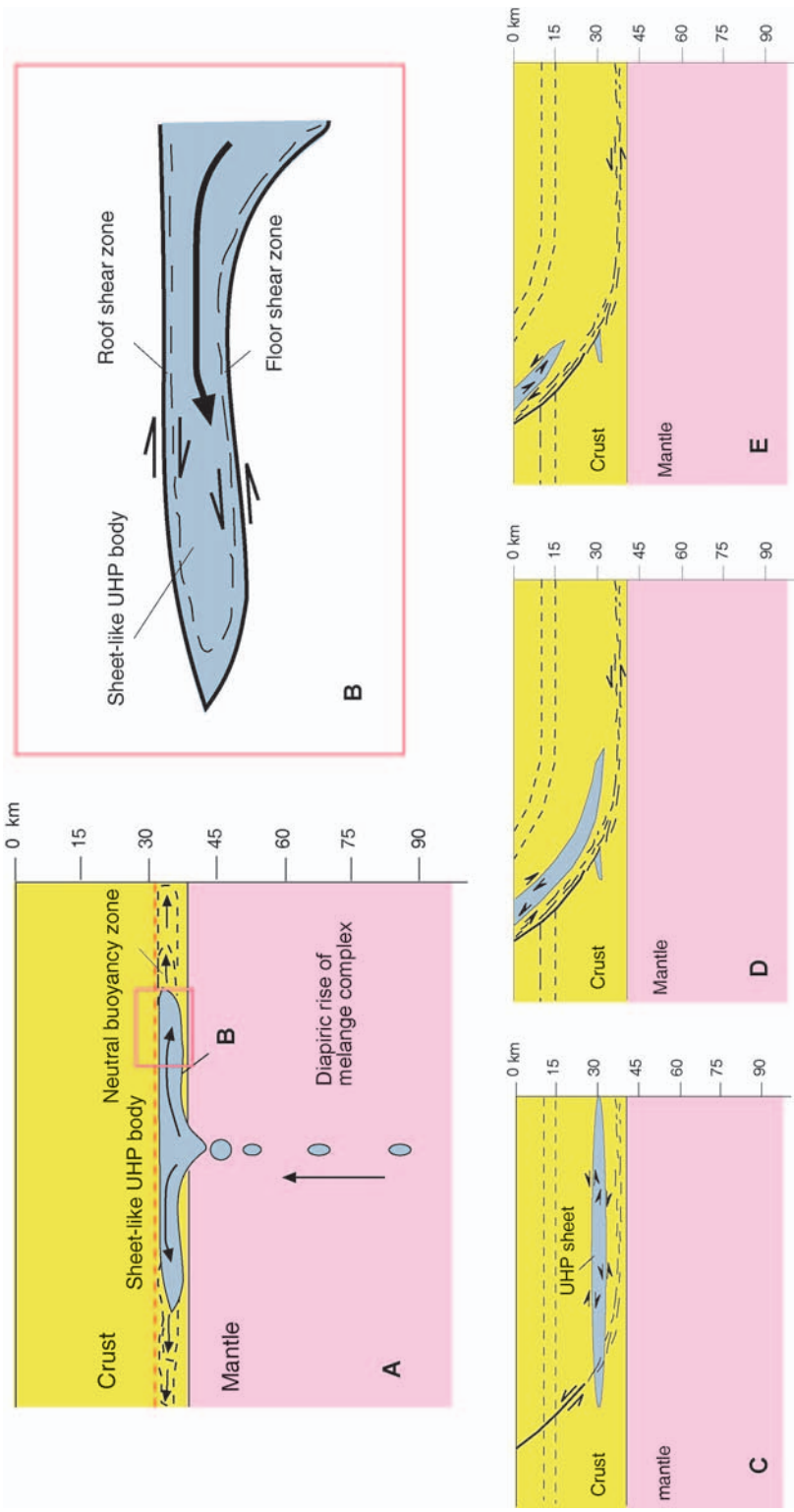


FIG. 17. Possible kinematic processes associated with emplacement and subsequent deformation and exhumation of the North Qaidam UHP metamorphic rocks. A. Sheet-like UHP rock mass was emplaced into the lower crust when it reaches neutral buoyancy zone. B. The UHP rock sheet spreads laterally and produces opposite sense of shear at the top and bottom to form the roof and floor shear zones. In this model, we suggest that the Luliang Shan detachment is a roof shear zone placing lower grade rocks over higher grade rocks. C–F. Later contractional deformation and motion on thrusts carried the UHP metamorphic terranes to the Earth's surface. The contractional event does not have to be related to the UHP metamorphism, which explains the long residence time for the UHP rocks in North Qaidam.

We believe that transporting UHP metamorphic rocks from mantle depths to the lower and middle crust via diapiric flow, either during oceanic or continental subduction, may be more widespread than previously thought. The reason that diapiric-flow processes are difficult to recognize is that the magmatic arc regions commonly lack large-magnitude crustal shortening that leads to transport of lower crustal rocks to the surface. This is in strong contrast to the continent-continent collisional orogens such as the Himalaya and the Qinglin Dabie systems where a large magnitude of crustal shortening and associated erosion during continental collision allow extensive exposure of the lower crustal rocks, which increases the chance of these special rocks to be observed at the Earth's surface.

### *Nature of the Luliang Shan detachment*

As we describe above, the Luliang Shan detachment cannot be interpreted as a North American Cordillera-style extensional detachment fault, because we could not locate any potential breakaway zone for the structure. In addition, the fault is folded under high-temperature conditions (>300°C), suggesting that its formation may have been a transient event during a protracted contractional event in the middle and lower crust. The variable lineation trends along the tectonic contact suggest that the surface was accommodating deformation of two nonrigid rock masses. These observations and our interpretation that the North Qaidam UHP metamorphic rocks were derived from subduction complexes or a tectonically eroded continental margin lead us to suggest that the Luliang Shan detachment was an accommodation fault assisting the emplacement of a UHP metamorphic rock mass into the overlying lower crust of the Qilian arc. The latter may—or may not—be floored by continental basement. We envision that the diapiric bodies were spreading laterally as they reached the neutral buoyancy zones in the lower crust (Fig. 17A). The spreading may have created opposite senses of shear on the top and bottom of the UHP sheet to form the roof and floor shear zones (Fig. 17B). We suggest that the Luliang Shan detachment is a *roof shear zone* placing lower grade rocks over higher grade rocks. A slab of UHP metamorphic rocks bounded on top and bottom by shear zones with opposite sense of slip has been observed in may UHP terranes around the world, which have been used as evidence to support the wedge extrusion model (e.g., Kaneko et al., 2000). The exposure of the North Qaidam UHP metamorphic terrane may have been eventually induced by Devonian crustal shortening and denudation during the final collision of the Qilian arc with the North China craton (Li et al., 1978; Yin and Nie, 1996; Yin and Harrison, 2000) (Figs. 6 and 17C–17E).

## Conclusions

North Qaidam UHP metamorphism occurred between 495 and 420 Ma, coeval with regional arc magmatism and spatially overlapping the arc. The protolith of UHP rocks is a mixture of continental, mafic, and ultramafic materials that were subducted along with an oceanic slab to a depth >70 km. The subducted materials were transported across the mantle wedge and eventually emplaced into the base of a coeval arc. We hypothesize that the exhumation of the UHP rocks was accomplished by diapiric flow. A quantitative scheme simulating the inferred diapiric flow allows us to track the P-T and T-t paths of individual diapirs. Using this model, we are able to determine the possible thermal and mechanical conditions under which the observed P-T paths from North Qaidam were achieved. In the context of our quantitative diapiric-flow model, the large variation of P-T conditions across the North Qaidam UHP belt and contrasting P-T paths between individual UHP terranes imply diverse geotherms and mantle rheology across the mantle wedge during the early Paleozoic Qilian subduction. In particular, the coldest P-T paths with a peak temperature of ~700°C requires the effective viscosity to be two orders of magnitude lower than those determined for dry olivine. This inference is consistent with the experimental results showing the strength of olivine aggregates can be lowered for two to three orders of magnitude in the presence of water.

## Acknowledgments

The idea of diapiric flow for UHP metamorphism during oceanic subduction was first conceived by one of the authors in 2000 while mapping in the Luliang Shan area (AY). He has received stimulating discussions with Scott Paterson, Brad Hacker, Sue Kay, J. G. Liou, Chris Mattinson, and Gary Ernst while presenting the idea in the past few years at the University of Southern California, UC Santa Barbara, Cornell University, and Stanford University. We are particularly grateful to Professor J. G. Liou (Louie) for his generous support and strong

encouragement at the start of the project. This research is supported by U.S. National Science Foundation grant EAR-0337191.

## REFERENCES

Balance, P. F., Scholl, D. W., Vallier, T. L., Stevenson, A. J., Ryan, H., and Herzer, R. H., 1989, Subduction of a late Cretaceous seamount of the Louisville ridge at the Tonga trench—a model of normal and accreted tectonic erosion: Tectonics, v. 8, p. 953–962.

Baldwin, S. L., Monteleone, B. D., Webb, L. E., Fitzgerald, P. G., Grove, M., and Hill, E. J., 2004, Pliocene eclogite exhumation at plate tectonic rates in eastern Papua New Guinea: Nature, v. 431, p. 263–267.

Bally, A. W., Chou, I.-M., Clayton, R., Eugster, H. P., Kidwell, S., Meckel, L. D., Ryder, R. T., Watts, A. B., and Wilson, A. A., 1986, Notes on sedimentary basins in China—report of the Amerian Sedimentary Basins delegation to the People's Republic of China: USGS Open File Report 86327, 108 p.

Barth, A. P., and Schneiderman, J. S., 1996, A comparison of structures in the Andean orogen of northern Chile and exhumed midcrustal structures in southern California, USA: An analogy in tectonic style?: International Geology Review, v. 38, p. 1075–1085.

Burchfiel, B. C., Deng, Q., Molnar, P., Royden, L. H., Wang, Y., Zhang, P., and Zhang, W., 1989, Intracrustal detachment with zones of continental deformation: Geology, v. 17, p. 748–752.

Carslaw, H. S., and Jeager J. C., 1959, Conduction of heat in solids: Oxford, UK, Clarendon Press, 510 p.

Chemenda, A. I., Burg, J. P., and Mattauer, M., 2000, Evolutionary model of the Himalaya-Tibet system: Geopoem based on new modeling, geological, and geophysical data: Earth and Plantary Science Letters, v. 174, p. 397–409.

Chemenda, A. I., Mattauer, M., and Bokun, A. N., 1996, Continental subduction and a mecahnism for exhumation of high-pressure metamorphic rocks: New modeling and field data from Oman: Earth and Planetary Science Letters, v. 143, p. 173–182.

Chen, X. H., Yin, A, Gehrels, G. E., Cowgill, E. S., Grove, M., Harrison, T. M., and Wang, X. F., 2003, Two phases of Mesozoic north-south extension in the eastern Altyn Tagh Range, northern Tibetan plateau: Tectonics, v. 22, article no. 1053.

Chopin, C., 1984, Coesite and pure pyrope in high-grade blueschists of the western Alps: A first record and some consequences: Contribution to Mineralogy and Petrology, v. 86, p. 107–118.

Chopin, C., 2003, Ultrahigh-pressure metamorphism: Tracing continental crust into the mantle: Earth and Planetary Science Letters, v. 212, p. 1–14.

Cloos, M., 1982, Flow mélange: Numerical modeling and geologic constraints on their origin in the Franciscan subduction complex, California: Geological Society of America Bulletin, v. 93, p. 330–345.

Cloos, M., 1993, Lithospheric buoyancy and collisional orogenesis: Subduction of oceanic plateau, continental margins, island arcs, spreading ridges, and seamounts: Geological Society of America Bulletin, v. 105, p. 715–737.

Cloos, M., and Shreve, R., 1988a, Subduction-channel flow model of prism accretion, mélange formation, sediment subduction, and subduction erosion at convergent plate margins, 1. Background and description: Pure and Applied Geophysics, v. 128, p. 455–499.

Cloos, M., and Shreve, R., 1988b, Subduction-channel flow model of prism accretion, mélange formation, sediment subduction, and subduction erosion at convergent plate margins, 2. Implications and discussions: Pure and Applied Geophysics, v. 128, p. 501–545.

Cowgill, E.S., 2001, Tectonic evolution of the Altyn Tagh and the Western Kunlun Shan, northern Tibetan Plateau: Unpubl. Ph.D. thesis, University of California, Los Angeles.

Cowgill, E. S., Yin, A., Harrison, T. M., and Wang, X. F., 2003, Reconstruction of the western Altyn Tagh fault: Constraints from U-Pb ion microprobe zircon geochronology: Journal of Geophysical Research, v. 108, article no. 2346.

Coleman, R. G., and Wang, X., 1995, Ultrahigh-pressure metamorphism: Cambridge, UK, Cambridge University Press, 528 p.

Cui, J. W and 11 others, 1998, Altyn Tagh fault system: Beijing, China, Geological Publishing House, 249 p.

Crowell, J. C., 1981, An outline of the tectonic history of southeastern California, *in* Ernst, W. G., ed., The geotectonic development of California: Rubey Volume 1: Englewood Cliffs, NJ: Prentice-Hall, p. 583–600.

CSBS (Chinese State Bureau of Seismology), The Altyn Tagh active fault system: Beijing, China, Seismology Publishing House.

Darby, B. J., Ritts, B. D., Yue, Y. J., and Meng, Q. R., 2005, Did the Altyn Tagh fault extend beyond the Tibetan Plateau?: Earth and Planetary Science Letters, v. 240, p. 425–435.

Davies, J. H., and van Blanckenburg, F., 1995, Slab breakoff: A model of lithosphere detachment and its test in the magmatism and deformation of collisional orogens: Earth and Planetary Science Letters, v. 129, p. 85–102.

de Sigoyer, J., Chavagnac, V., Blichert-Toft, J., Villa, I. M., Luais, B., Buillot, S., Cosca, M., and Mascle, G., 2000, Dating the Indian continental subduction and collisional thickening in the northwest Himalaya: Multichronology of the Tso Morari eclogites: Geology, v. 28, p. 487–490.

Dewey, J. F., Ryan, P. D., and Andersen, T. B., 1993, Orogenic uplift and collapse, crustal thickness, fabrics, and metamorphic phase changes: The role of eclogites, *in* Prichard, H. M., et al., eds., Magmatic processes

and plate tectonics: Geological Society [London] Special Publication 76, p. 325–343.

Dobretsov, N. L., 2000, Collision processes in Paleozoic foldbelts of Asia and exhumation mechanisms: Petrology, v. 8, p., 403–427.

Ducea, M. N., 2001, The California Arc: Thick granitic batholiths, eclogitic residues, lithospheric-scale thrusting, and magmatic flare-ups: GSA Today, v. 11, no. 11, p. 4–10.

Ducea, M. N., and Saleeby, J. B., 1996, Buoyancy sources for a large, unrooted mountain range, the Sierra Nevada, California: Evidence from xenolith thermobarometry: Journal of Geophysical Research, v. 101, p. 8229–8244.

Ducea, M. N., and Saleeby, J. B., 1998, The age and origin of a thick mafic-ultramafic keel from beneath the Sierra Nevada batholith: Contribution Mineralogy and Petrology, v. 133, p. 169–185.

Ernst, W. G., and Liou, J. G., 1995, Contrasting plate tectonic styles of the Qinling-Dabie-Sulu and Franciscan metamorphic belts: Geology, v. 23, p. 253–256.

Ernst, W. G., and Liou, J. G., 2000a, Ultrahigh-pressure metamorphism and geodynamics in collision-type orogenic belts: Columbia, MD, Bellwether Publishing, Ltd., Geological Society of America, International Book Series, v. 4,, 293 p.

Ernst, W. G., and Liou, J. G., 2000b, Overview of UHP metamorphism and tectonics in well-studied collisional orogens, *in* Ernst, W. G., and Liou, J. G., eds., Ultrahigh-pressure metamorphism and geodynamics in collision-type orogenic belts: Columbia, MD, Bellwether Publishing, Ltd., Geological Society of America, International Book Series, v. 4, p. 3–19.

Ernst, W. G., and Peacock, S. M., 1996, A thermotectonic model for preservation of ultrahigh-pressure phases in metamorphosed continental crust, *in* Gray, G. E., Scholl, D. W., Kirby, S. H., and Platt, J. P., eds., Subduction: Top to bottom: Washington, DC, American Geophysical Union, Geophysical Monograph 96, p. 171–178.

Fang, X. M., Garzione, C., Van der Voo, R., Li, J. J., and Man, M. J., 2003, Flexural subsidence by 29 Ma on the NE edge of Tibet from the magentostritigraphy of Linxia basin, China: Earth and Planetary Science Letters, v. 210, p. 545–560.

Gansu BGMR (Gansu Bureau of Geology and Mineral Resources), 1991, Regional geology of Gansu Province: Beijing, China, Geological Publishing House (in Chinese with English abstract).

Gehrels, G. E., Yin, A., and Wang, X. F., 2003a, Detritatl-zircon geochronology of the northeastern Tibetan Plateu: Geological Society of America Bulletin, v. 115, p. 881–896.

Gehrels, G. E., Yin, A., and Wang, X. F., 2003b, Magmatic history of the northeastern Tibetan Plateau: Journal of Geophysical Research, v. 108, article no. 2423.

George, A. D., Marshallsea, S. J., Wyrwoll, K.-H., Chen, J., and Lu, Y. C., 2001, Miocene cooling in the northern Qilian Shan, northeastern margin of the Tibetan Plateau, revealed by apatite fission-track and vitrinite-reflectance analysis: Geology, v. 29, p. 939–942.

Gerya, T. V., and Yuan, D. A., 2003, Rayleigh-Taylor instabilities from hydration and melting propel "cold plumes" at subduction zones: Earth and Planetary Science Letters, v. 212, p. 47–62.

Gerya, T. V., Yuan, D.A., and Sevre, E. O. D., 2004, Dynamical causes for incipient magma chambers above: Geology, v. 32, p. 89–92.

Gilder, S., Chen, Y., and Sen, S., 2001, Oligo-Miocene magnetostratigraphy and rock magnetism of the Xishuigou section, Subei (Gansu Province, western China) and implications for shallow inclinations in Central Asia: Journal of Geophysical Research, v. 106 (B12), p. 30,505–30,521.

Gilotti, J. A., and Ravna, E. J. K., 2002, First evidence for ultrahigh-pressure metamorphism in the North-East Greenland Caledonides: Geology, v. 30, p. 551–554.

Hacker, B. R., and Liou, J. G., 1998, When continents collide: Geodynamics and geochemistry of ultrahigh-pressure Rocks: Dordrecht, The Netherlands, Kluwer Academic Publishers, 323 p.

Hacker, B., Luffi, P., Lutkov, V., Minaev, V., Ratschbacher, L., Plank, T., Ducea, M., Patino-Douce, A., McWilliams, M., and Metcalf, J., 2005, Near-ultrahigh pressure processing of continental crust: Miocene crustal xenoliths from the Pamir: Journal of Petrology, v. 46, p. 1661–1687.

Hacker, B. R., Ratschbacher, L, Webb, L., McWilliams, M. O., Ireland, T., Calvert, A., Dong, S. W., Wenk, H.-R., and Chateigner, D., 2000, Exhumation of ultrahigh-pressure continental crust in east central China: Late Triassic–Early Jurassic tectonic unroofing: Journal Geophysical Research, v. 105, p. 13,339–12,364.

Hall, C. A., Jr., 1991, Geology of the Point Sur–Lopez Point region, Coast Ranges, California: A part of the Southern California allochthon: Geological Society of America Special Paper 266, 40 p.

Hall, P. S., and Kincaid, C., 2001, Diapiric flow at subduction zones: A recipe for rapid transport: Science, v. 292, p. 2472–2475.

Hirth, G., and Kohlstedt, D. L., 1996, Water in the oceanic upper crust mantle: Implications for rheology, melt extraction, and the evolution of the lithosphere: Earth and Planetary Science Letters, v. 144, p. 93–108.

Hirth, G., and Tullis, J., 1992, Dislocation creep regimes in quartz: Journal of Structural Geology, v, 14, p. 145–159.

Huo, Y. L, and Tan, S. D., 1995, Exploration case history and petroleum geology in Jiuquan continental basin: Beijing, China, Petroleum Industry Press, 211 p.

Hsu, K., and 15 others, 1995, Tectonic evolution of the Tibetan Plateau: A working hypothesis based on the

archipelago model of orogenesis: International Geology Review, v. 37, p. 473–508.

Huang, H., Huang, Q., and Ma, Y., 1996, Geology of the Qaidam Basin and its petroleum prediction:, Beijing, China, Geological Publishing House (in Chinese).

Jahn, B.-M., 1999, Sm-Nd isotope tracer study of UHP metamorphic rocks: Implications for continental subduction and collisional tectonics: International Geology Review, v. 41, p. 859–885.

Jacobson, C. E., Oyarzabal, F. R., and Haxel, G. B., 1996, Subduction and exhumation of the Pelona-Orocopia-Rand schists, southern California: Geology, v. 24, 547–550.

Jolivet, M., Brunel, M., Seward, D., Xu, Z., Yang, J., Roger, F., Tapponnier, P., Malavieille, J., Arnaud, N., and Wu, C., 2001, Mesozoic and Cenozoic tectonics of the northern edge of the Tibetan Plateau: Fission-track constraints: Tectonophysics, v. 343, p. 111–134.

Kaneko, Y., Maruyama, S., Terabayashi, M., Yamamoto, H., Ishikawa, M., Anma, R., Parkinson, C. D., Ota, T., Nakajima, Y., and Katayama, I., 2000, Geology of the Kotchetav UHP-HP metamorphic belt, northern Kazakhstan: The Island Arc, v. 9, p. 264–283.

Kapp, P., Yin, A., Manning, C. E., Murphy, M., Harrison, T. M., Spurlin, M., Ding, L., Deng, X. G., and Wu, C. M., 2000, Blueschist-bearing metamorphic core complexes in the Qiangtang block reveal deep crustal structure of northern Tibet: Geology, v. 28, p. 19–22.

Kapp, P., Murphy, M. A., Yin, A., Harrison, T. M., Ding, L., and Guo, J. H., 2003a, Mesozoic and Cenozoic tectonic evolution of the Shiquanhe area of western Tibet: Tectonics, v. 22, p. 1029.

Kapp, P, Yin, A., Manning, C. E., Harrison, T. M., Taylor, M. H., and Ding, L., 2003b, Tectonic evolution of the early Mesozoic blueschist-bearing Qiangtang metamorphic belt, central Tibet: Tectonics, v. 22, p. 1043.

Kohn, M. J., and Parkinson, C. D., 2002, Petrologic case for Eocene slab breakoff during the Indo-Asian: Geology, v. 30, p. 591–594.

Kirby, S. H., 1983, Rheology of the lithosphere: Reviews of Geophysics, v. 21, p. 1458–1487.

Lardeaux, J. M., Ledru, P., Daniel, I., and Duchene, S., 2001, The Variscan French Massif Central—a new addition to the ultrahigh pressure metamorphic "club": Exhumation processes and geodynamic consequences: Tectonophysics, v. 332, p. 143–167.

Leech, M. L., Singh, S., Jain, A. K., Klemperer, S. L., and Manickavasagam, R. M., 2005, The onset of India-Asia continental collision: Early, steep subduction required by the timing of UHP metamorphism in the western Himalaya: Earth and Planetary Science Letters, v. 234, p. 83–97.

Li, C. Y., Liu, Y., Zhu, B., Feng, Y. M., and Wu, H. C., 1978, Structural evolution of Qinling and Qilian Shan, *in* Scientific papers on geology and international exchange: Beijing, China, Geologic Publishing House, p. 174–197 (in Chinese with English abstract).

Li, H. K., Lu, S. N., Zhao, F. Q., and Yu, H. F., 1999, Determination and significance of the coesite eclogite on the Yuqia River on the northern margin of the Qaidam basin: Geosciences, v. 13, p. 43–50 (in Chinese with English abstract).

Liou, J. G., Tsujimori, T., Zhang, R. Y., Katayama, I., and Maruyama, S., 2004, Global UHP metamorphism and continental subduction/collision: The Himalayan model: International Geology Review, v. 46, p. 1–27.

Liou, J. G., Zhang, R. Y., Wang, X. M., Eide, E. A., Ernst, W. G., and Maruyama, S., 1996, Metamorphism and tectonics of high-pressure and ultra-high pressure belts in the Dabie-Sulu region, China, *in* Yin, A., and Harrison, T. M., eds., The tectonic evolution of Asia: Cambridge, UK, Cambridge University Press, p. 300–344.

Lister, G. S., and Davis, G. A., 1989, The origin of metamorphic core complexes and detachment faults formed during Tertiary continental extension in the northern Colorado River region, USA: Journal of Structural Geology, v. 11, p. 65–94.

Liu, Z. Q., 1988, Geologic map of the Qinghai–Xiang Plateau and its neighboring regions (scale at 1:1,500,000): Beijing, China, Geologic Publishing House and Chengdu Institute of Geology and Mineral Resources.

Mahon, K. I., Harrison, T. M., and Drew, D. A., 1988, Ascent of a granitoid diapir in a temperature varying medium: Journal of Geophysical Research, v. 93, p. 1174–1188.

Mancktelow, N. S., 1995, Nonlithostatic pressure during sediment subduction and development and exhumation of high-pressure metamorphic rocks: Journal of Geophysical Research, v. 100, p. 571–583.

Manning, C. E., Menold, C. A., and Yin, A., 2001, Metamorphism and exhumation of ultrahigh-pressure eclogites and gneisses, north Qaidam, China [abs.]: Geological Society of America, Abstracts with Programs, v. 33, no. 6, p. 252.

Marsh, B. D., 1979, Island arc development: Some observations, experiments, and speculations: Journal of Geology, v. 87, p. 687–713.

Marsh, B. D., 1982, On the mechanics of igneous diapirism, stoping, and zone melting: American Journal of Sciences, v. 282, p. 808–855.

Marsh, B. D., and Kantha, L. H., 1978, On the heat and mass transfer from an ascending magma: Earth and Planetary Science Letters, v. 39, p. 435–443.

Maruyama, S., Liou, J. G., and Zhang, R. Y, 1994, Tectonic evolution of the ultrahigh-pressure (UHP) and high-pressure (HP) metamorphic belts from central China: The Island Arc, v. 3, p. 112–121.

Mattinson, C. G., Wooden, J. L., Liou, J. G., Bird, D. K., and Wu, C. L., 2006, Geochronology and tectonic significance of Middle Proterozoic granitic orthogneiss, North Qaidam HP/UHP terrane, Western China: Mineralogy and Petrology, v. 88, p. 227–241.

Mei, S., and Kohlstedt, D. L., 2000, Influence of water on plastic deformation of olivine aggregates, 2. Dislocation creep regime: Journal of Geophysical Research, v. 105, p. 21,471–21,481.

Menold, C. A., Manning, C. E., and Yin, A., 2001, Metamorphism and exhumation of very high pressureeclogites, North Qaidam, China: EOS (Transactions of American Geophysical Union), v. 82, p. 47.

Menold, C. A., Manning, C. E., and Yin, A., 2003a, P-T evolution of the North Qaidam HP-UHP terrane, Western China: Torino, Italy, European Mineralogical Union School and Symposium on UHP metamorphism.

Menold, C. A., Manning, C. E., and Yin, A., 2003b, Metamorphism and exhumation of very high pressure eclogites, North Qaidam, China: American Geophysical Union, Fall Meeting.

Meyer, B., Tapponnier, P., Bourjot, L., Metivier, F., Gaudemer, Y., Peltzer, G., Shunmin, G., and Zhitai, C., 1998, Crustal thickening in Gansu-Qinghai, lithospheric mantle subduction, and oblique, strike-slip controlled growth of the Tibet Plateau: Geophysical Journal International, v. 135, p. 1–47.

Nie, S., Yin, A., Rowley, D. B., and Jin, Y., 1994, Exhumation of the Dabie Shan ultra-high pressure metamorphic rocks and accumulation of the Songpan-Ganzi flysch sequence: Geology, v. 22, p. 999–1002.

O'Brien, P. J., Zotov, N., Law, R., Khan, M. A., and Jan, M. Q., 2001, Coesite in Himalayan eclogite and implications for models of India-Asia collision: Geology, v. 29, p. 435–438.

Okay, A. I., and Sengör, A. M. C., 1992, Evidence for intracontinental thrust-related exhumation of the ultrahigh-pressure rocks in China: Geology, v. 20, p. 411–414.

Pares, J. M., Van der Voo, R., Downs, W. R., Yan, M., and Fang, X. M., 2003, Northeastward growth and uplift of the Tibetan Plateau: Magnetostratigraphic insights from the Guide: Journal of Geophysical Research, v. 108 (B1), p. 2017.

Parkinson, C. D., Miyazaki, K., Wakita, K., Barber, A. J., and Carswell, D. A., 1998, An overview and tectonic synthesis of the pre-Tertiary very-high-pressure metamorphic and associated rocks of Java, Sulawesi, and Kalimantan, Indonesia: Island Arc, v. 7, nos. 1–2, p. 184–200.

Peacock, S. M., and Wang, K., 1999, Seismic consequences of warm versus cold subdution metamorphism: Examples from southwest and northeast Japan: Science, v. 286, p. 937–939.

Qinghai BGMR (Qinghai Bureau of Geology and Mineral Resources), 1991, Regional geology of Qinghai Province: Beijing, China, Geological Publishing House (in Chinese with English abstract).

Ranalli, G., Pellegrini, R., and D'Offizi, S., 2000, Time dependence of negative buoyancy and the subduction of continental lithosphere: Journal of Geodynamics, v. 30, p. 539–555.

Regenauer-Lieb, K., Yuan, D. A., and Branlund, J., 2001, The initiation of subduction: Criticality by addition of water?: Science, v. 294, p. 578–580.

Rieser, A. B., Neubauer, F., Liu, Y. J., and Ge, X. H., 2005, Sandstone provenance of north-western sectors of the intracontinental Cenozoic Qaidam basin, western China: Tectonic vs. climatic control: Sedimentary Geology, v. 177, p. 1–18.

Ritts, B. D., and Biffi, U., 2000, Magnitude of post-Middle Jurassic Baojocian displacement on the central Altyn Tagh fault system, northwest China: Geological Society of America Bulletin, v. 112, p. 61–74.

Ryan, P. D., 2001, The role of deep basement during continent-continent collision: A review, *in* Miller, J. A., et al., eds., Continental reactivation and reworking: Geological Society [London] Special Publication 184, p. 39–55.

Saleeby, J., 2003, Segmentation of the Laramide slab—evidence from the southern Sierra Nevada region: Geological Society of America Bulletin, v. 115, no. 6, p. 655–668.

Searle, M,. Hacker, B. R., and Bilham, R., 2001, The Hindu Kush seismic zone as a paradigm for the creation of ultrahigh-pressure diamond- and coesite-bearing continental rocks: Journal of Geology, v. 109, p. 143–153.

Sengör, A. M. C., and Natal'in, B. A., 1996, Paleotectonics of Asia: Fragments of a synthesis, *in* Yin, A., and Harrison, T. M., eds., The tectonics of Asia: New York, NY, Cambridge University Press, p. 486–640.

Shreve, R. L., and Cloos, M., 1986, Dynamics of sediment subduction, mélange formation, and prism accretion: Journal of Geophysical Research, v. 86, p. 11,522–11,535.

Smith, D. C., 1984, Coesite in clinopyroxene in the Caledonides and its implications for geodynamics: Nature, v. 310, p. 641–644.

Sobel, E. R., 1999, Basin analysis of the Jurassic–Lower Cretaceous southwest Tarim basin, NW China: Geological Society of America Bulletin, v. 111, p. 709–724.

Sobel, E. R., and Arnaud, N. A., 1999, Possible middle Paleozoic suture in the Altyn Tagh, northwest China: Tectonics, v. 18, p. 64–74.

Song, T., and Wang, X., 1993, Structural styles and stratigraphic patterns of syndepositional faults in a contractional setting: Examples from Qaidam basin, northwestern China: American Association of Petroleum Geologists Bulletin, v. 77, p. 102–117.

Song, S. G., Yang, J. S., Xu, Z. Q., Liou, J. G., and Shi, R. D., 2003, Metamorphic evolution of the coesite-bearing ultrahigh-pressure terrane in the North Qaidam, Northern Tibet, NW China: Journal of Metamorphic Geology, v. 21, p. 631–644.

Song, S. G., Zhang, L. F., Niu, Y. L., Su, L., Jian, P., and Liu, D. Y., 2005, Geochronology of diamond-bearing zircons from garnet peridotite in the North Qaidam UHPM belt, northern Tibetan Plateau: A record of

complex histories from oceanic lithosphere subduction to continental collision: Earth and Planetary Science Letters, v. 234, p. 99–118.

Song, S. G., Zhang, L. F., Niu, Y. L., Su, L, Song, B. A., and Liu, D. Y, 2006, Evolution from oceanic subduction to continental collision: A case study from the northern Tibetan Plateau based on geochemical and geochronological data: Journal of Petrology, v. 47, p. 435–455.

Taylor, M., Yin, A., Ryerson, F. J., Kapp, P., and Ding, L., 2003, Conjugate strike-slip faulting along the Bangong-Nujiang suture zone accommodates coeval east-west extension and north-south shortening in the interior of the Tibetan Plateau: Tectonics, v. 22, article no. 1044.

Usui, T., Nakamura, E., Kobayashi, K., Maruyama, S., and Helmstaedt, H., 2003, Fate of the subducted Farallon plate inferred from eclogite xenoliths in the Colorado Plateau: Geology, v. 31, p. 589–592.

van Blanckenburg, F., and Davies, J.H., 1995, Slab breakoff: A model for syncollisional magmatism and tectonics in the Alps: Tectonics, v. 14, p. 120–131.

van den Beukel, J., 1992, Some thermomechanical aspect of the subduction of continental lithosphere: Tectonics, v. 11, p. 316–329.

van Keken, P. E., Kiefer, B., and Peacock, S. M., 2002, High-resolution models of subduction zones: Implications for mineral dehydration reactions and the transport of water into the deep mantle: Geochemistry, Geophysics, Geosystems, v. 3, p. 1056.

Vannucchi, P., Scholl, D. W., Meschede, M., and McDougall-Reid, K., 2001, Tectonic erosion and consequence collapse of the Pacific margin of Costa Rica: Combined implications from ODP Leg 170, seismic offshore data, and regional geology of the Nicaoya Peninsula: Tectonics, v. 20, p. 649–668.

Vincent, S. J., and Allen, M. B., 1999, Evolution of the Minle and Chaoshui basins, China: Implications for Mesozoic strike-slip basin formation in Central Asia: Geological Society of America Bulletin, v. 111, p. 725–742.

von Huene, R., and Lallemand, S., 1990, Effect of erosion along the Japan and Peru convergent margins: Geological Society of America Bulletin, v. 102, p. 704–720.

Wakita, K., 2000, Cretaceous accretionary-collision complexes in central Indonesia: Journal of Asian Earth Sciences, v. 18, p. 739–749.

Wang, E., 1997, Displacement and timing along the northern strand of the Altyn Tagh fault zone, northern Tibet: Earth and Planetary Science Letters, v. 150, p. 55–64.

Wang, E. C., and Burchfiel, B. C., 2004, Late cenozoic right-lateral movement along the Wenquan fault and associated deformation: Implications for the kinematic history of the Qaidam Basin, northeastern Tibetan Plateau: International Geology Review, v. 46, p. 861–879.

Wang, Q. C., and Cong, B. L., 1999, Exhumation of UHP terranes: A case study from the Dabie Mountains, eastern China: International Geology Review, v. 41, p. 994–1004.

Wang, X. M., Wang, B. Y., Qiu, Z. X., Xie, G. P., Xie, J. Y., Downs, W., Qiu, Z. D., and Deng, T., 2003, Danghe area (western Gansu, China): Biostratigraphy and implications for depositional history and tectonics of northern Tibetan Plateau: Earth and Planetary Science Letters, v. 208, p. 253–269.

Weinberg, R. F., and Podladchikov, Y., 1994, Diapiric ascent of magmas through power law crust and mantle: Journal of Geophysical Research, v. 99, p. 9543–9559.

Whitmarsh, R. B., Manatschal, G., and Minshull, T. A., 2001, Evolution of magma-poor continental margins from rifting to seafloor spreading: Nature, v. 413, p. 150–154.

Yang, J. J., Zhu, H., and Deng, J. F., 1994, The discovery of garnet peridotite in Northern Qaidam Mountains, and its significance: Acta Petrologica et Mineralogica, v. 13, p. 97–105 (in Chinese with English abstract).

Yang, J. S., Xu, Z. Q., Li, H. B., Wu, C. L., Shi, R. D., and Zhang, Z. X., 1998, The discovery of eclogite in the northern margin of Qaidam basin, China: Chinese Science Bulletin, v. 43, p. 1544–1548 (in Chinese).

Yang, J. S., Xu, Z. Q., Song, S. G., Wu, C. L., Shi, R. D., Zhang, J. X., Wan, Y. S., Li, H. B., Jin, X. C., and Jolivet, M., 2000, Discovery of eclogite in Dulan, Qinghai Province and its significance for studying the HP-UHP metamorphic belt along the central orogenic belt of China: Acta Geologica Sinica, v. 74, p. 156–168.

Yang, J. S., Song, S. G., Xu, Z. Q., Liu, F. L., Maruyama, S., Liou, J. G., Zhang, J. X., Wu, C. L., Li, H. B., and Shi, R. D., 2001, Discovery of coesite in the north Qaidam Caledonian ultrahigh-high-pressure (UHP-HP) metamorphic belt on the northeastern Qinghai-Tibet Plateau, *in* Proceedings of the 11th Annual V. M. Goldschmidt Conference, p. 3088.

Ye, S., Bialas, J., Flueh, E. R., Stavenhagen, A., von Huene, R., Leandro, G., and Hinz, K., 1996, Crustal structure of the middle American trench off Costa Rica from wide-angle seismic data: Tectonics, v. 15, p. 1006–1021.

Yin, A., 2002, A passive-roof thrust model for the emplacement of the Orocopia-Pelona Schist in Southern California: Geology, v. 30, p. 183–186.

Yin, A., 2004, Gneiss domes and gneiss dome systems, *in* Whitny, D. L., Teysser, C., and Siddway, C. S., eds., Gneiss domes in orogeny: Boulder, CO, Geological Society of America Special Paper 380, p. 1–14.

Yin, A., 2006, Cenozoic evolution of the Himalayan orogen as constrained by along-strike variations of structural geometry, exhumation history, and foreland sedimentation: Earth Science Reviews, v. 76, p. 1–131.

Yin, A., and Harrison, T. M., 2000, Geologic evolution of the Himalayan-Tibetan orogen: Annual Review of Earth Planetary Sciences, v. 28, p. 211–280.

Yin, A., Manning, C. E., and Menold, C., 2001, Tectonic erosion, diapiric flow, and emplacement of UHP rocks during oceanic subduction: Origin of North Qaidam UHP gneiss [abs.]: Geological Society of America, Abstracts with Programs, v. 33, no. 6, p. 207.

Yin, A., and Nie, S. Y., 1993, Development of the Tan-Lu fault as a transform system during collision of the north and south China blocks, east-central China: Tectonics, v. 12, p. 801–813.

Yin, A., and Nie, S., 1996, A Phanerozoic palinspastic reconstruction of China and its neighboring regions, *in* Yin, A., and Harrison, T. M., eds., The tectonic evolution of Asia: New York, NY, Cambridge University Press, p. 442–485.

Yin, A., Rumelhart, P. E., Butler, R., Cowgill, E., Harrison, T. M., Foster, D. A., Ingersoll, R. V., Zhang, Q., Zhou, X. Q., Wang, X. F., and Raza, A., 2002, Tectonic history of the Altyn Tagh fault in northern Tibet inferred from Cenozoic sedimentation: Geological Society of America Bulletin, v. 114, p. 1257–1295.

Yue, Y. J., and Liou, J. G., 1999, Two-stage evolution model for the Altyn Tagh fault: Geology, v. 27, p. 227–230.

Yue, Y. J., Ritts, B. D., and Graham, S. A., 2001, Initiation and long-term slip history of the Altyn Tagh fault: International Geology Review, v. 43, p. 1087–1093.

Yue, Y. J., Ritts, B. D., Hanson, A. D., and Graham, S. A., 2004, Sedimentary evidence against large strike-slip translation on the Northern Altyn Tagh fault, NW China: Earth and Planetary Science Letters, v. 228, p. 311–323.

Zhang, J., Zhang, Z., Xu, Z., Yang, J., and Cui, J., 2001, Petrology and geochronology of eclogites from the western segment of the Altyn Tagh, northwestern China: Lithos, v. 56, p. 187–206.

Zhang, J. X., Yang, J. S., Mattinson, C. G., Xu, Z. Q., Meng, F. C., and Shi, R. D., 2005, Two contrasting eclogite cooling histories, North Qaidam HP/UHP terrane, western China: Petrological and isotopic constraints: Lithos, v. 84, p. 51–76.

Zhang, X. M., Liou, J. G., and Coleman, R. G., 1984, An outline of the plate tectonics of China: Geological Society of America Bulletin, v. 95, p. 295–312.

Zhang, Y. C., 1997, Prototype analysis of petroliferous basins in China: Nanjing, China, Nanjing University Press, 450 p.

Zindler, A., and Hart, S., 1986, Chemical geodynamics: Annual Review of Earth and Planetary Sciences, v. 14, p. 493–571.

Zonenshain, L. P., Kuzmin, M. I., and Natapov, L. M., 1990, Geology of the USSR: A plate-tectonic synthesis: Washington DC, American Geophysical Union, Geodynamics Series, no. 21, 242 p.